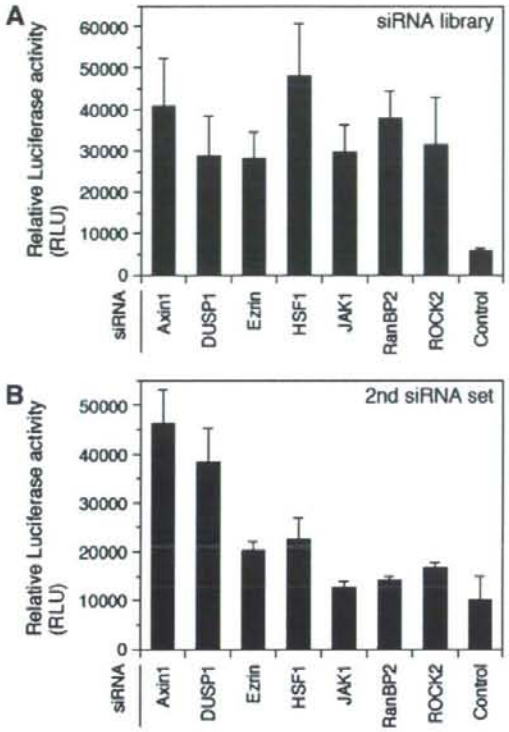

Fig. 2. siRNAs against Axin1 and DUSP1 reproducibly enhanced the HIV-1 gene expression. J111 cells were transfected with the siRNAs included in siRNA mini-library (A) or the second set of siRNAs (B) directed against the indicated target gene. Forty-eight hours after siRNA-transfection, the cells were transfected with pNL-Luc-envCT and pRL-TK. Forty-eight hours after the transfection of HIV-1 proviral construct, the cells were harvested, and the both of firefly and *Renilla* luciferase activities were measured, as described in Materials and methods. The firefly luciferase activity was normalized to the *Renilla* luciferase activity. Data are represented by means and standard deviations (error bars) of four independent experiments.

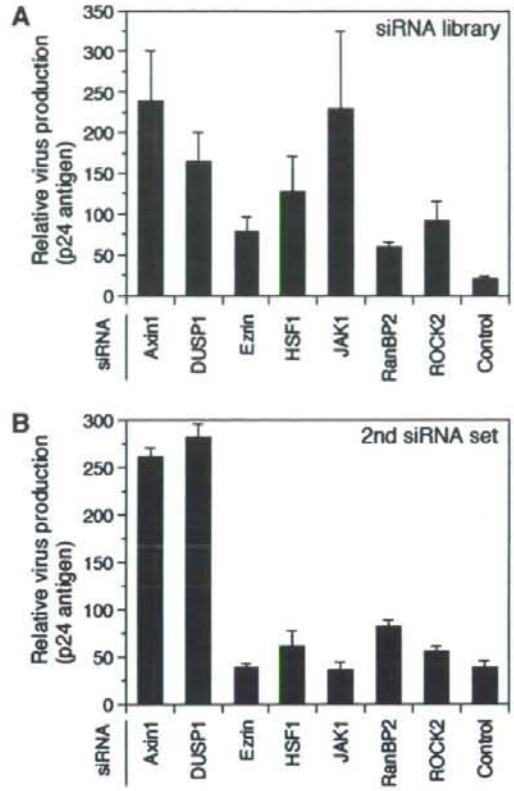

Fig. 3. siRNAs against Axin1 and DUSP1 reproducibly enhanced the HIV-1 replication at the late phase(s) of viral life cycle. J111 cells were transfected with siRNA, and then transfected with pNL-Luc-envCT and pRL-TK, as described in the legend of Fig. 2. Forty-eight hours after the transfection of HIV-1 proviral construct, the level of p24 antigens in the cell culture supernatants was measured, as described in Materials and methods. Data are represented by means and standard deviations (error bars) of four independent experiments.

in our assay system (data not shown). We next carried out the experiments using the second set of siRNAs directed against the different gene region of each target gene to confirm the gene-specific effects of siRNAs. The results showed that second set of the siRNAs against Axin1 and DUSP1, but not JAK1, HSF-1, ROCK2, RanBP2, and Ezrin, significantly enhanced the levels of luciferase activity (Fig. 2B) and p24 antigen (Fig. 3B). We also performed the experiments using the third set of siRNAs against JAK1, HSF-1, ROCK2, RanBP2, and Ezrin, but the results showed that those siRNAs did not enhanced the late phase of HIV-1 replication (data not shown). These results suggested that siRNAs against JAK1, HSF-1, ROCK2, RanBP2, and Ezrin non-specifically enhanced the HIV-1 replication. We carried out the sequential transfection of the cells with siRNA and HIV-1 molecular clone for studying the late phase of the HIV-1 life cycle. Although, we found no particular cell death in siRNA-transfected cells by WST-1 test (data not shown), the multiple transfection process may cause the physiological stress to the cells, and we consider that this is a part of reasons why some siRNAs showed such a high level of non-specific effects. Taken together with these results, we may conclude that the siRNAs against Axin1 and DUSP1 could enhance the HIV-1 replication at the late phase of viral life cycle, as a gene-specific manner. The target sequences of siRNAs against Axin1 and DUSP1 included in siRNA mini-library are 5′-TGGATACCTGCCGACCTTAAATG-3′ and 5′-TACCTTATGAGGACTAATCGAGT-3′, respectively.

DUSP1 is known as the mitogen-activated protein kinase (MAPK) phosphatase (MKP)-1, and is a negative regulator of MAPK signal transduction pathways [39] as well as of innate immune responses [40,41]. On the other hand, Axin1 is known as the regulator of WNT signaling pathway [42,43]. Our data suggest that Axin1 and DUSP1 negatively regulate the late phase of HIV-1 replication. The

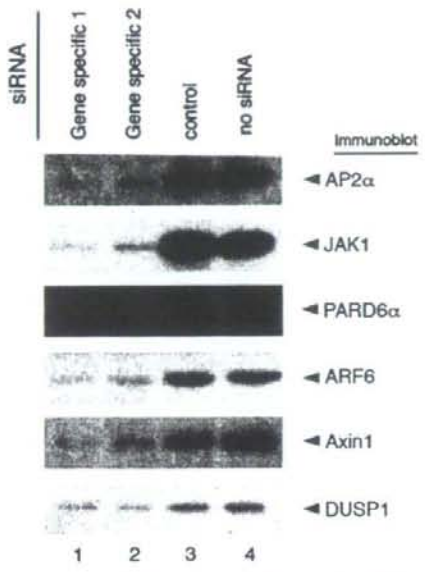

Fig. 4. Two sets of siRNAs against AP2α, ARF6, PARD6α, JAK1, Axin1, and DUSP1 suppressed the expression levels of target gene products. J111 cells were transfected with two sets of siRNA against indicated target gene (lanes 1 and 2), control siRNA (lane 3) or MOCK-transfected (lane 4). Then, the cells were subjected to immunoblot analysis. Indicated target gene products were immuno-stained using appropriate antibodies, as described in Materials and methods.

siRNA against Axin1 and DUSP1 reproducibly increased both of the luciferase activity in the cells transfected with HIV-1 proviral construct (Fig. 2) and the level of p24 antigen in the cell culture supernatant (Fig. 3), suggesting that these host factors may affect the transcription and/or translation step(s) in HIV-1 life cycle.

Study on protein levels of six host factors in siRNA-transfected cells. Finally, we confirmed the RNAi effects of siRNAs against six host factors using immunoblot analysis. The results showed that two sets of siRNAs against AP2α, ARF6, PARD6α, JAK1, Axin1, and DUSP1 reproducibly reduced the levels of target proteins (Fig. 4).

We revealed in this study that six host factors play roles as the negative regulators for HIV-1 replication. The precise mechanisms by which the host factors regulate viral replication are still unknown at moment. We are now underway to determine the target step(s) of those host factors in the HIV-1 life cycle.

Acknowledgments

This work was supported in part by the program of Founding Research Center for Emerging and Reemerging Infectious Diseases launched by a project commissioned by the Ministry of Education, Cultures, Sports, Science and Technology (MEXT) of Japan, a Health Sciences Research Grant from the Ministry of Health, Labor and Welfare of Japan, and the 21st Century COE program (Combined Program on Microbiology and Immunology) from the Japan Society for the Promotion of Science. The manuscript was proofread by Medical English Service (Kyoto, Japan).

Appendix A. Supplementary data

Supplementary data associated with this article can be found, in the online version, at doi:10.1016/j.bbrc.2007.05.173.

References

[1] A.P. Rice, J.T. Kimata, Cellular cofactors and HIV-1 infection in vivo, Future Virol. 1 (2006) 337–347.
[2] Y.-H. Zheng, N. Lovsin, B.M. Peterlin, Newly identified host factors modulate HIV replication, Immunol. Lett. 15 (2005) 225–234.
[3] Y. Feng, C.C. Broder, P.E. Kennedy, E.A. Berger, HIV-1 entry cofactor: functional cDNA cloning of a seven-transmembrane, G-protein-coupled receptor, Science 272 (1996) 872–877.
[4] H. Deng, R. Liu, W. Ellmeier, S. Choe, D. Unutmaz, M. Burkhart, P. Di Marzio, S. Marmon, R.E. Sutton, C.M. Hill, C.B. Davis, S.C. Peiper, T.J. Schall, D.R. Littman, N.R. Landau, Identification of a major co-receptor for primary isolates of HIV-1, Nature 381 (1996) 661–666.
[5] T. Dragic, V. Litwin, G.P. Allaway, S.R. Martin, Y. Huang, K.A. Nagashima, C. Cayanan, P.J. Maddon, R.A. Koup, J.P. Moore, W.A. Paxton, HIV-1 entry into CD4+ cells is mediated by the chemokine receptor CC-CKR-5, Nature 381 (1996) 667–673.
[6] E. Sokolskaja, J. Luban, Cyclophilin, TRIM5, and innate immunity to HIV-1, Curr. Opin. Microbiol. 9 (2006) 404–408.
[7] M. Stremlau, C.M. Owens, M.J. Perron, M. Kiessling, P. Autissier, J. Sodroski, The cytoplasmic body component TRIM5α restricts HIV-1 infection in old world monkeys, Nature 427 (2004) 848–853.
[8] A novel CDK9-associated C-type cyclin interacts directly with HIV-1 Tat and mediates its high-affinity, loop-specific binding to TAR RNA, Cell 92 (1998) 451–462.
[9] B.R. Cullen, Nuclear mRNA export: insights from virology, Trends Biochem. Sci. 28 (2003) 419–424.
[10] Y.-H. Zheng, H.-F. Yu, B.M. Peterlin, Human p32 protein relieves a post-transcriptional block to HIV replication in murine cells, Nat. Cell Biol. 5 (2003) 611–618.
[11] S.M. Elbashir, J. Harborth, W. Lendeckel, A. Yalcin, K. Weber, T. Tuschl, Duplexes of 21-nucleotide RNAs mediated RNA interference in cultured mammalian cells, Nature 411 (2001) 494–498.
[12] M. Kameoka, S. Nukuzuma, A. Itaya, Y. Tanaka, K. Ota, K. Ikuta, K. Yoshihara, RNA interference directed against poly(ADP-ribose) polymerase 1 efficiently suppresses human immunodeficiency virus type 1 replication in human cells, J. Virol. 78 (2004) 8931–8934.
[13] A. Adachi, H.E. Gendelman, S. Koenig, T. Folks, R. Willey, A. Rabson, M.A. Martin, Production of acquired immunodeficiency syndrome-associated retrovirus in human and nonhuman cells transfected with an infectious molecular clone, J. Virol. 59 (1986) 284–291.
[14] B.K. Chen, K. Saksela, R. Andino, D. Baltimore, Distinct modes of human immunodeficiency virus type 1 proviral latency revealed by superinfection of nonproductively infected cell lines with recombinant luciferase-encoding viruses, J. Virol. 68 (1994) 654–660.
[15] R.I. Connor, B.K. Chen, S. Choe, N.R. Landau, Vpr is required for efficient replication of human immunodeficiency virus type-1 in mononuclear phagocytes, Virology 206 (1995) 935–944.
[16] R.A.M. Fouchier, B.E. Meyer, J.H.M. Simon, U. Fischer, M.H. Malim, HIV-1 infection of non-dividing cells: evidence that the amino-terminal basic region of the viral matrix protein is important for Gag processing but not for post-entry nuclear import, EMBO J. 16 (1997) 4531–4539.

[17] M. Kinomoto, M. Yokoyama, H. Sato, A. Kojima, T. Kurata, K. Ikuta, T. Sata, K. Tokunaga, Amino acid 36 in the human immunodeficiency virus type 1 gp41 ectodomain controls fusogenic activity: Implications for the molecular mechanism of viral escape from a fusion inhibitor, J. Virol. 79 (2005) 5996–6004.
[18] S.D. Connor, S.L. Schmid, Regulated portals of entry into the cells, Nature 422 (2003) 37–44.
[19] F. Nakatsu, H. Ohno, Adaptor protein complexes as the key regulators of protein sorting in the post-golgi network, Cell Struct. Funct. 28 (2003) 419–429.
[20] R.A. Kahn, A.G. Gilman, The protein cofactor necessary for ADP-ribosylation of Gs by cholera toxin in itself a GTP-binding protein, J. Biol. Chem. 261 (1986) 7906–7911.
[21] J.G. Donaldson, R.D. Klausner, ARF: a key regulatory switch in membrane traffic and organella structure, Curr. Opin. Cell Biol. 6 (1994) 527–532.
[22] J. Moss, M. Vaughan, Structure and function of ARF proteins: activators of cholera toxin and critical components of intracellular vesicular transport processes, J. Biol. Chem. 270 (1995) 12327–12330.
[23] H.A. Brown, S. Gutowski, C.R. Moomaw, C. Slaughter, P.C. Sternweis, ADP-ribosylation factor, a small GTP-dependent regulatory protein, stimulates phospholipase D activity, Cell 75 (1993) 1137–1144.
[24] C. D'Souza-Schorey, G. Li, M.I. Colombo, P.D. Stahl, A regulatory role for ARF6 in receptor-mediated endocytosis, Science 267 (1995) 1175–1178.
[25] Y. Altschuler, S. Liu, L. Katz, K. Tang, S. Hardy, F. Brodsky, G. Apodaca, K. Mostov, ADP-ribosylation factor 6 and endocytosis at the apical surface of Madin-Darby canine kidney cells, J. Cell Biol. 147 (1999) 7–12.
[26] N. Naslavsky, R. Weigert, J.G. Donaldson, Convergence of non-clathrin- and clathrin-derived endosomes involves Arf6 inactivation and changes in phosphoinositides, Mol. Biol. Cell 14 (2003) 417–431.
[27] O. Paleotti, E. Macia, F. Luton, S. Klein, M. Partisani, P. Chardin, T. Kirchhausen, M. Franco, The small G-protein Arf6GTP recruits the AP-2 adaptor complex to membranes, J. Biol. Chem. 280 (2005) 21661–21666.
[28] M. Boge, S. Wyss, J.S. Bonifacino, M. Thali, A membrane-proximal tyrosine-based signal mediates internalization of the HIV-1 envelope glycoprotein via interaction with the AP-2 clathrin adaptor, J. Biol. Chem. 273 (1998) 15773–15778.
[29] J. Daecke, O.T. Fackler, M.T. Dittmar, H.-G. Kräusslich, Involvement of clathrin-mediated endocytosis in human immunodeficiency virus type 1 entry, J. Virol. 79 (2005) 1581–1594.
[30] J.J. Rose, K. Janvier, S. Chandrasekhar, R.P. Sekaly, J.S. Bonifacino, S. Venkatesan, CD4 down-regulation by HIV-1 and simian immunodeficiency virus (SIV) Nef proteins involves both internalization and intracellular retention mechanisms, J. Biol. Chem. 280 (2005) 7413–7426.
[31] Y.-J. Jin, C.Y. Cai, X. Zhang, H.-T. Zhang, J.A. Hirst, S.J. Burakoff, HIV Nef-mediated CD4 down-regulation is adaptor protein complex 2 dependent, J. Immunol. 175 (2005) 3157–3164.
[32] M. Batonick, M. Favre, M. Boge, P. Spearman, S. Höning, M. Thali, Interaction of HIV-1 gag with the clathrin-associated adaptor AP-2, Virology 342 (2005) 190–200.
[33] A.D. Blagoveshchenskaya, L. Thomas, S.F. Feliciangeli, C.-H. Hung, G. Thomas, HIV-1 Nef downregulates MHC-I by a PACS-1- and PI3K-regulated ARF6 endocytic pathway, Cell 111 (2002) 853–866.
[34] V. Maréchal, F. Clavel, J.M. Heard, O. Schwartz, Cytosolic Gag p24 as an index of productive entry of human immunodeficiency virus type 1, J. Virol. 72 (1998) 2208–2212.
[35] G. Joberty, C. Petersen, L. Gao, I.G. Macara, The cell-polarity protein Par6 links Par3 and atypical protein kinase C to Cdc42, Nature Cell Biol. 2 (2000) 531–539.
[36] Y. Noda, R. Takeya, S. Ohno, S. Naito, T. Ito, H. Sumimoto, Human homologues of the Caenorhabditis elegans cell polarity protein PAR6 as an adaptor that links the small GTPases Rac and Cdc42 to atypical protein kinase C, Genes Cells 6 (2001) 107–119.
[37] C.E. Samuel, Antiviral actions of interferons, Clin. Microbiol. Rev. 14 (2001) 778–809.
[38] A. Takaoka, H. Yanai, Interferon signaling network in innate defence, Cell. Microbiol. 8 (2006) 907–922.
[39] A. Farooq, M.-M. Zhou, Structure and regulation of MAPK phosphatases, Cell. Signal. 16 (2004) 769–779.
[40] H. Chi, S.P. Barry, R.J. Roth, J.J. Wu, E.A. Jones, A.M. Bennett, R.A. Flavell, Dynamic regulation of pro- and anti-inflammatory cytokines by MAPK phosphatase 1 (MKP-1) in innate immune responses, Proc. Natl. Acad. Sci. USA 103 (2006) 2274–2279.
[41] K.V. Salojin, I.B. Owusu, K.A. Millerchip, M. Potter, K.A. Platt, T. Oravecz, Essential role of MAPK phosphatage-1 in the negative control of innate immune responses, J. Immunol. 176 (2006) 1899–1907.
[42] M.D. Gordon, R. Nusse, Wnt signaling: multiple pathways, multiple receptors, and multiple transcription factors, J. Biol. Chem. 281 (2006) 22429–22433.
[43] K. Willert, K.A. Jones, Wnt signaling: is the party in the nucleus? Genes Dev. 20 (2006) 1394–1404.

Separate elements are required for ligand-dependent and -independent internalization of metastatic potentiator CXCR4

Yuko Futahashi,[1] Jun Komano,[1,4] Emiko Urano,[1] Toru Aoki,[1,2] Makiko Hamatake,[1] Kosuke Miyauchi,[1] Takeshi Yoshida,[3] Yoshio Koyanagi,[3] Zene Matsuda[1] and Naoki Yamamoto[1,2]

[1]AIDS Research Center, National Institute of Infectious Diseases, 1-23-1 Toyama, Shinjuku, Tokyo 162-8640; [2]Department of Molecular Virology, Tokyo Medical and Dental University, 1-5-45, Yushima, Bunkyo-ku, Tokyo 113-8519; [3]Laboratory of Viral Pathogenesis, Institute for Virus Research, Kyoto University, 53 Shougoin-kawahara machi, Sakyou-ku, Kyoto 606-8507, Japan

(Received September 17, 2006/Revised November 3, 2006/Accepted November 11, 2006/Online publication January 19, 2007)

The C-terminal cytoplasmic domain of the metastatic potentiator CXCR4 regulates its function and spatiotemporal expression. However, little is known about the mechanism underlying constitutive internalization of CXCR4 compared to internalization mediated by its ligand, stromal cell-derived factor-1 alpha (SDF-1α)/CXCL12. We established a system to analyze the role of the CXCR4 cytoplasmic tail in steady-state internalization using the NP2 cell line, which lacks endogenous CXCR4 and SDF-1α. Deleting more than six amino acids from the C-terminus dramatically reduced constitutive internalization of CXCR4. Alanine substitution mutations revealed that three of those amino acids Ser^{344} Glu^{345} Ser^{346} are essential for efficient steady-state internalization of CXCR4. Mutating Glu^{345} to Asp did not disrupt internalization, suggesting that the steady-state internalization motif is S(E/D)S. When responses to SDF-1α were tested, cells expressing CXCR4 mutants lacking the C-terminal 10, 14, 22, 31 or 44 amino acids did not show downregulation of cell surface CXCR4 or the cell migration induced by SDF-1α. Interestingly, however, we identified two mutants, one with E344A mutation and the other lacking the C-terminal 17 amino acids, that were defective in constitutive internalization but competent in ligand-promoted internalization and cell migration. These data demonstrate that ligand-dependent and -independent internalization is genetically separable and that, between amino acids 336 and 342, there is a negative regulatory element for ligand-promoted internalization. Potential involvement of this novel motif in cancer metastasis and other CXCR4-associated disorders such as warts, hypogammaglobulinemia, infections and myelokathexis (WHIM) syndrome is discussed. (*Cancer Sci* 2007; 98: 373–379)

The chemokine receptor CXCR4 is a class-A G protein-coupled receptor (GPCR; reviewed in [1,2]) and its natural ligand is stromal cell-derived factor-1 alpha (SDF-1α)/CXCL12. CXCR4 also serves as the receptor for HIV type 1 (HIV-1). Many cell types express CXCR4, including peripheral blood lymphocytes, monocytes-macrophages, thymocytes, dendritic cells, endothelial cells, epithelium-derived tumor cells, microglial cells, neurons and hematopoietic stem cells. CXCR4 plays multiple biological roles from promoting development of neuronal networks to regulating migration of leukocytes, cerebellar granule cells and hematopoietic stem cells.[3–8] Analysis of knockout mice indicates that the CXCR4/SDF-1α system is essential for maintenance of hematopoiesis and intestinal vascularization.[9,10]

The CXCR4/SDF-1α system also functions in pathological processes, including autoimmune diseases, cancer progression and metastasis, and AIDS caused by HIV-1. Recently, metastasis of breast cancer cells was found to be regulated by the CXCR4/SDF-1α axis.[5] Similarly, other studies have found that metastasis of other malignancies was controlled by the CXCR4/SDF-1α system, including colon carcinoma[11] non-small cell lung cancer[12] and prostate cancer.[13] These observations suggest that the CXCR4/SDF-1α axis is a potential target for metastatic cancer therapy.

Warts, hypogammaglobulinemia, infections and myelokathexis (WHIM) syndrome is a rare combined immunodeficiency characterized by an unusual form of neutropenia. It is reported that the CXCR4 cytoplasmic tail is mutated and often truncated in WHIM syndrome.[14] Thus, determining the biochemical activity of the CXCR4 cytoplasmic tail should facilitate understanding of the pathogenesis of WHIM syndrome as well as suggest ways to control cancer metastasis.

Following SDF-1α binding, CXCR4 is activated, triggering multiple signaling cascades via Gα or β-arrestin 2 (reviewed in[15]). To desensitize activated CXCR4, the G protein-coupled receptor kinase (GRK) is recruited and phosphorylates serine residues on the CXCR4 cytoplasmic tail, thereby inactivating Gα-mediated signal. Simultaneously, CXCR4 is internalized in a clathrin-dependent manner. β-arrestin 2 competes with Gα for CXCR4 binding and can initiate signal transduction independent from Gα. β-arrestin 2 can also induce clathrin-dependent CXCR4 endocytosis. Thus, cell surface levels of CXCR4 transiently decrease after agonist binding but, several hours later, surface levels of CXCR4 return to normal. Most internalized CXCR4 is transported to lysosomes and degraded, but some internalized CXCR4 is recycled. It is reported that amino acids within the cytoplasmic tail are required for agonist-dependent endocytosis of CXCR4.[16–18]

By contrast, it is unclear how steady-state cell surface levels of CXCR4 are maintained in the absence of SDF-1α. Although cell surface levels of CXCR4 could be regulated at the transcriptional level, it is likely that primary regulation occurs post-translationally. Given that the cell surface levels of CXCR4 are positively correlated with cancer cells' ability to metastasize,[5,19] understanding the post-translational behavior of CXCR4 is likely to shed light on metastatic processes. Historically, cells expressing endogenous CXCR4 have been used for analysis of CXCR4 trafficking. However, as is the case with many G protein-coupled receptors (GPCR), CXCR4 trafficking is influenced by spontaneous oligomerization in the absence of ligand.[20–22] Thus, previous observations might not correctly model phenotypes seen in CXCR4 mutants.

In the present study, we analyzed the contribution of the cytoplasmic tail to the post-translational trafficking of CXCR4 in a cell line lacking both endogenous CXCR4 and SDF-1α. Using genetic approaches, we identified two amino acid motifs within the CXCR4 cytoplasmic tail; one that positively regulates

*To whom correspondence should be addressed. E-mail:ajkomano@nih.go.jp

doi: 10.1111/j.1349-7006.2007.00388.x

spontaneous ligand-independent internalization and the other that negatively regulates ligand-dependent CXCR4 internalization.

Materials and methods

Cells. The glioblastoma cell line NP2, human embryonic kidney (HEK) 293T, and HeLa, cells were maintained in RPMI-1640 (Sigma, Tokyo, Japan) supplemented with 10% FBS (Japan Bioserum, Tokyo, Japan), penicillin and streptomycin (Invitrogen, Tokyo, Japan). All cell lines were incubated at 37°C in the humidified 5% CO_2 atmosphere.

Plasmids. Full-length CXCR4 cDNA was amplified from a plasmid kindly provided by Dr Shioda[23] using the following primers: sense, 5′-ACCGGTGCCACCATGGAGGGGATCAGT-ATATACACTTCAG-3′, and antisense, 5′-AGATCTCGCTGGA-GTGAAAACTTGAAGACTCAGACTC-3′. CXCR4 lacking the cytoplasmic tail (d-44) was amplified using the same sense primer and the antisense primer, 5′-AGATCTTGGCTCCAAGGAAA-GCATAGAGGATGGG-3′. Polymerase chain reaction (PCR) fragments were cloned into the *Age* I-*Bgl* II sites of pEGFP-C2 (Clontech, Palo Alto, CA, USA) to create pCXCR4 FL and pCXCR4 d-44, respectively. To construct pCXCR4 FL- and d-44-GFP, the *Sna* BI-*Bgl* II fragments from pCXCR4 FL and d-44 were cloned into the *Sna* BI-*Bgl* II sites of pEGFP-N2, respectively (Clontech). To construct pCXCR4 FL- and d-44-GFP flag, the *Sna* BI-*Bgl* II fragments from pCXCR4 FL and d-44 were cloned into the *Sna* BI-*Bgl* II sites of pEGFP-flag in which the following annealed oligonucleotides had been inserted into the *Bsr* GI site of pEGFP-N2: forward, 5′-GTACGACTAC-AAAGACGATGACGACTATAAGTAAGC-3′, and reverse, 5′-GGCCGCTTACTTATAGTCGTCATCGTCTTTGTAGTC-3′. To construct pCMMP CXCR4 FL- and d-44-GFP, pCXCR4 FL- and d-44-GFP were digested with *Not* I, blunted using T4 DNA polymerase, and further digested with *Age* I. The Age *I*-blunted *Not* I fragments of both constructs were cloned into the pCMMP eGFP plasmid that had been digested with *Bam* HI, blunted with T4 DNA polymerase, and digested with *Age* I. pCMMP CXCR4 FL- and d-44-GFP-flag were constructed using the same strategy. CXCR4 deletion and point mutants were PCR-amplified using the sense primer 5′-ACCGGTGCCACCATGGAGGGGATCAGTG-TGAAAACTTGAAGACTCAGACTC-3′ and the following reverse primers: d-6, 5′-AAGCTTGAGCTCGAGATCTCAG-ACTCAGACTCAGTGGAAAC-3′; d-10, 5′-AAGCTTGAGC-TCGAGATCTCAGTGGAAACAGATGAATGTCC-3′; d-14, 5′-AAGCTTGAGCTCGAGATCTCTGAATGTCCACCTCGC-TTTCC-3′; d-17, 5′-AAGCTTGAGCTCGAGATCTCACCTC-GCTTTCCTTTGG-3′; d-22, 5′-AAGCTTGAGCTCGAGATCT-CGGAGAGGATCTTGAGGCTGGACC-3′; d-31, 5′-AAGCTT-GAGCTCGAGATCTCGCTCACAGAGGTGAGTGCGTGC-3′; E343A, 5′-CGAGATCTCGCTGGAGTGAAAACTTGAAGAC-TCAGACGCAGTGGAAACAGATGAATGTC-3′; S344A, 5′-CGAGATCTCGCTGGAGTGAAAACTTGAAGACTCAGCCT-CAGTGGAAACAGATGAATGTC-3′; E345A, 5′-CGAGATC-TCGCTGGAGTGAAAACTTGAAGACGCAGACTCAGTGGA-AACAGATGAATGTC-3′; S346A, 5′-CGAGATCTCGCTGGA-GTGAAAACTTGAAGCCTCAGACTCAGTGGAAACAGATG-AATGTC-3′; S347E, 5′-CGAGATCTCGCTGGAGTGAAAA-CTTTCAGACTCAGACTCAGTGGAAACAGATGAATGTC-3′; H350E, 5′-CGAGATCTCGCTGGACTCAAAACTTGAAGAC-TCAGACTCAGTGGAAACAGATGAATGTC-3′; S347E/H350E, 5′-CGAGATCTCGCTGGACTCAAAACTTTCAGACTCAGA-CTCAGTGGAAACAGATGAATGTC-3′; and E343/345D, 5′-CGAGATCTCGCTGGAGTGAAAACTTGAAGAGTCAGAGT CAGTGGAAACAGATGAATGTC-3′. The PCR fragments were cloned into the *Age* I-*Bgl* II sites of pCMMP CXCR4 FL-GFP-flag, replacing wild-type with mutant CXCR4. Protein expression of each mutant in 293T cells was verified by Western blot analysis.

Immunoblotting. Immunoblotting was performed as described.[24,25] The primary antibody was anti-green fluorescent protein (GFP) polyclonal antibody (Beckton Dickinson, San Jose, CA, USA). The secondary probe was EnVision+ (Dako, Glostrup, Denmark). Signals were visualized with an LAS3000 imager (Fuji Film, Tokyo, Japan) after treating the membranes with the Lumi-Light Western Blotting Substrate (Roche Diagnostics GmbH, Mannheim, Germany).

Flow cytometry. Cells were labeled with anti-CXCR4 antibodies recognizing the N-terminus conjugated with R-phycoerythrin (PE; 2B11, BD Pharmingen, San Diego, CA) or recognizing the second extracellular loop (12G5) conjugated with either PE or PE-Cy5 (Beckton Dickinson) for 30 min at 4°C. Cells were washed once with phosphate-buffered saline (PBS) supplemented with 1% FBS and analyzed by FACS Aria (Beckton Dickinson). To isolate GFP-expressing NP2 cells, cells were infected with murine leukemia virus (MLV)-based retroviral vectors as described.[25] Cells exhibiting similar green fluorescence intensities were gated and sorted by FACS Aria. Efficiency of internalization was measured by comparing mean fluorescence intensities for cell surface CXCR4 detected by a PE-labeled 2B11 monoclonal antibody before and after SDF-1α treatment (200 ng/mL, Peprotech EC, London, UK).

Microscopic analysis and imaging of cells. To judge a phenotype of a CXCR4 mutant, three independent scientists investigated the mutant cell phenotype under a fluorescent microscope (Olympus, Tokyo, Japan). Each scientist investigated more than 1000 cells for each mutant. More than 99% of cells of a mutant fell in the indicated phenotypic category. These phenotypes were unchanged for more than a year of continuous cultivation in tissue culture. For imaging, NP2 cells were grown on glass plates for more than 24 h, fixed in 4% formaldehyde in PBS for 5 min, stained with Hoechst 33258, mounted (Vectorshield, Vector Laboratories, Burlingame, CA, USA), and imaged using a confocal microscope META 510 (Carl Zeiss, Tokyo, Japan). A representative cell for each CXCR4 mutant carrying a wide cytoplasm was chosen such that the spatial resolution was high. The focal plane just above the glass surface was scanned with an optical thickness of approximately 1 μm. For the imaging of subcellular compartments, cells were incubated with either BODIPY TR ceramid, ER-Tracker Blue-White DPX, or Lysotracker Red DND-99 (Invitrogen) according to the manufacturer's protocol and imaged without fixation. Image brightness and contrast were processed by META510 software (Carl Zeiss). Unless noted, cells were imaged at ×630 magnification, the GFP signal was displayed in green, and Hoechst 33258-stained nuclei were blue. To visualize ligand-induced internalization, cells were treated with 200 ng/mL SDF-1α before fixation. The live cell imaging was performed using Leica DFC350FX system and the images were processed by FW4000 software (Leica Microsystems, Tokyo, Japan). Cells were plated on the glass-bottomed dish (Matsunami glass, Kishiwada, Japan) and incubated at 37°C in the humidified 5% CO_2 atmosphere during the monitoring.

Cell migration assay. Cell migration was measured using an HTS FluoroBlok Multiwell Insert System (8.0 μm pore size, BD Falcon) according to the manufacturer's protocol. For stimulation assays, cells were incubated without serum overnight before SDF-1α treatment (200 ng/mL). Cells were allowed to migrate overnight.

Statistical analysis. Significance of differences were determined by a Student's *t*-test. *P*-values less than 0.05 were considered significant.

RESULTS

Deleting 10 amino acids from the carboxyl end of CXCR4 alters the efficiency of constitutive internalization. Previous studies indicated that the cytoplasmic tail of CXCR4 amino acids 308–352 plays

doi: 10.1111/j.1349-7006.2007.00388.x

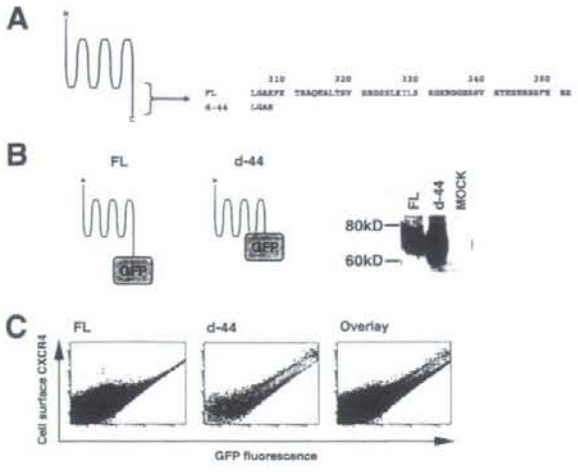

Fig. 1. The effect of stromal cell-derived factor-1 alpha (SDF-1α) treatment on NP2 cells expressing CXCR4 mutants. (a) Cells expressing d-17 were treated with SDF-1α, incubated at 37°C for the indicated times, fixed and imaged. The blue signal represents the Hoechst-stained nucleus. (Original magnification, ×630; bar, 10 μm). (b) FACS analysis to measure internalization efficiency of cell surface CXCR4 and mutant forms 2 h after SDF-1α exposure. The average and standard deviation from the indicated number of independent experiments are shown. Asterisks represent statistically significant difference from the FL levels ($P < 0.01$). (c) Cell migration assay to assess response of cells expressing CXCR4 and mutants to SDF-1α. The number of migrated cells in three to six randomly selected fields was counted and the average and standard deviation were calculated. (□) number of migrated cells in the absence of ligand; (■) migration in the presence of ligand. (*) statistically significant differences in the number of migrated cells between SDF-1α-untreated and -treated cells ($P < 0.01$).

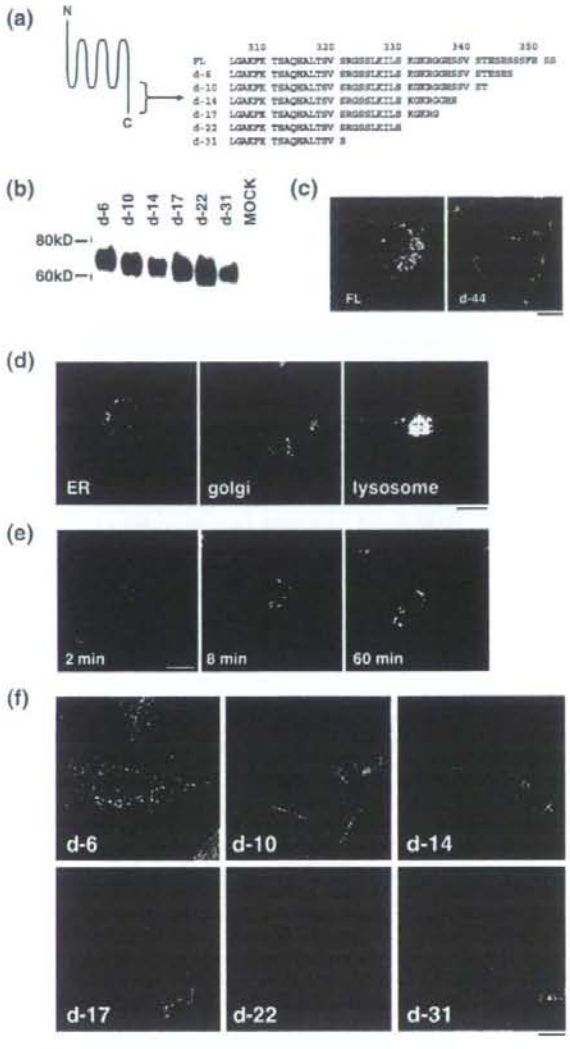

Fig. 2. Expression profiles of CXCR4 and a mutant with cytoplasmic tail deletion. (a) Schematic representation of CXCR4. The N-terminus CXCR4 is exposed in the extracellular space and the C-terminus is intracellular. Gray represents the lipid bilayer. The amino acid sequence of the cytoplasmic tail is shown. Residues in red are required for ligand-induced endocytosis. The CXCR4 d-44 mutant lacks amino acid 309–351. (b) Schematic representation and Western blot of FL and d-44 constructs. (c) Flow cytometry profiles of FL and d-44 expressed in 293T cells. The horizontal axis represents green fluorescence intensity indicative of green fluorescent protein (GFP)-tagged CXCR4 protein levels, and the vertical axis is PE-Cy5 fluorescence intensity, reflecting cell surface CXCR4 detected by the anti-CXCR4 antibody. GFP-positive cells expressing FL are colored in red (left) and those expressing d-44 in green (middle). The expressional differences between FL and d-44 is highlighted on the overlay plot (right).

a critical role in ligand-dependent internalization (Fig. 1a). Also, it has been shown in transfected cells that cell surface levels of CXCR4 lacking the cytoplasmic tail (equivalent to the d-44 mutant here) are higher than those of the full length, wild-type protein (hereafter designated FL), suggesting that the cytoplasmic tail of CXCR4 regulates steady-state internalization.[26,27] To confirm this, we constructed expression plasmids of CXCR4 FL and d-44 fused to GFP or GFP-FLAG at the C-terminus. Previous studies and data reported here indicated that CXCR4 function is not affected by this modification.[28] The expression of each construct was verified by Western blot analysis (Fig. 1b). Single cell-based quantitative analyzes revealed that the ratio of cell surface levels to the total amount of CXCR4 FL (Fig. 1c, left) was consistently lower than that of d-44 (Fig. 1c, middle) at any expression levels (Fig. 1c, right for the comparison). These data supported previous findings and demonstrate that constitutive internalization occurs at any level of CXCR4 expression.

To further examine the contribution of the cytoplasmic tail to post-translational trafficking of CXCR4, we devised a system utilizing the human NP2 glioma line: NP2 cells are flat and exhibit a large cytoplasmic space such that intracellular compartments can be well resolved under the microscope. NP2 cells also lack endogenous CXCR4[29] and SDF-1α (data not shown), both of which could potentially affect distribution of transduced CXCR4. However, NP2 cells are capable of appropriate signaling in response to CXCR4/SDF-1α interaction. We generated a series of CXCR4 deletion mutants lacking the cytoplasmic tail (Fig. 2a) and transduced them into NP2 cells using MLV vectors. Cells bearing similar green fluorescence intensities were collected by FACS sorter. The expression of each mutant was verified by Western blot analysis (Fig. 2b). Microscopic observations revealed that cells expressing FL were bordered by green fluorescence, and significant green fluorescence was detected in vesicular compartments of varying diameters lying close to the nucleus surrounding the nucleus (hereafter designated the FL phenotype, Fig. 2c, left). Vesicles around the nucleus were

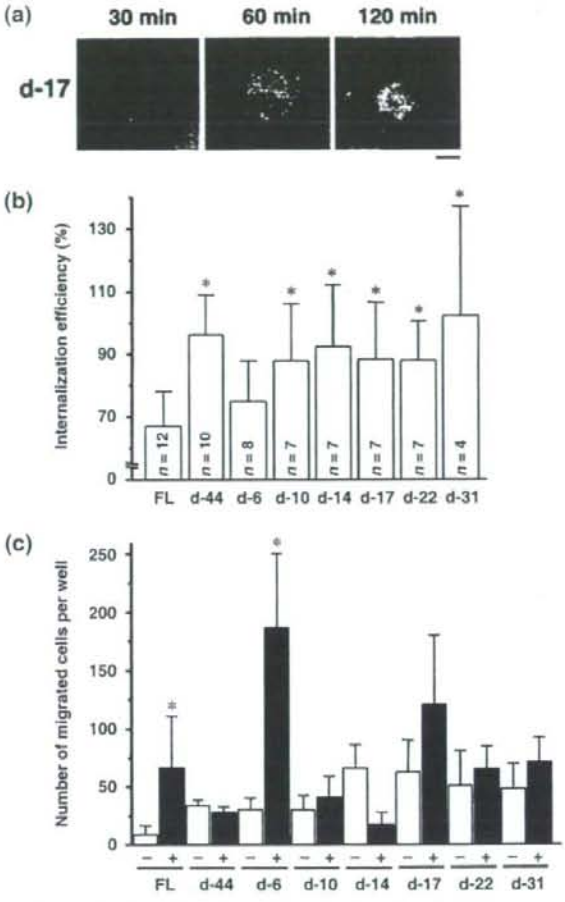

Fig. 3. Identification of the amino acids required for steady-state CXCR4 internalization. (a) Amino acid sequences of the cytoplasmic tail of FL and deletion mutants. Residues in red are required for ligand-induced endocytosis. (b) The protein expression of each mutant in 293T cells was verified by Western blot analysis. (c) Confocal micrographs of NP2 cells expressing FL and d-44 mutant proteins. The blue signal represents the Hoechst-stained nucleus. (Original magnification, ×630; bar, 10 μm.) (d) Confocal micrographs showing NP2 cells expressing CXCR4 FL stained with ER, Golgi, or lysosome organella markers. The organella marker signal is shown in red, the GFP signal is in green. The pixels that both red and green signals co-localized are shown in yellow. (Original magnification, ×630; bar, 10 μm.) (e) CXCR4 FL trafficking in the absence of SDF-1α in NP2 cells. Cell surface CXCR4 FL was labeled with an antibody conjugated with PE-Cy5 (red), incubated at 37°C for the indicated times, fixed and imaged. (Original magnification, ×630; bar, 10 μm.) (f) Confocal micrographs of NP2 cells expressing FL and mutant proteins. The intracellular vesicular green fluorescence reflecting steady-state internalization can be seen in the d-6 mutant. The blue signal represents the Hoechst-stained nucleus. (Original magnification, ×630; bar, 10 μm.)

mostly lysosomes, as demonstrated by fluorescent organella marker analyses in which cells expressing CXCR4 FL-GFP stained with the lysosomal marker yielded a substantial amount of co-localization signal. On the other hand, only a mall amount of co-localization signal was detected when the ER or Golgi markers were used (Fig. 2d), consistent with our biochemical fractionation (unpublished data) and previous publications.[16,27,28,30] The active constitutive internalization was visualized by labeling cell surface CXCR4 by PE-Cy5-conjugated monoclonal antibody followed by fluorescence imaging after cells were incubated at 37°C (Fig. 2e). The live cell imaging revealed that internalizing GFP-positive vesicles trafficked at an average velocity of 4.7 mm/h ($n = 15$), which is within the range of clathrin-dependent vesicular transport (2–20 mm/h), not that of caveolin-dependent vesicular transport (25–170 mm/h).[31–35] These data suggest that the FL is constitutively internalized from the cell surface to the cytoplasmic compartment. In sharp contrast, most green fluorescent signals from d-44 mutant-expressing cells were detected at the cell surface, and only a few small GFP-positive vesicles were seen in the cytoplasm near the nucleus (hereafter designated the d-44 phenotype, Fig. 2c, right). Similar observations were made in d-10, d-14, d-17, d-22 and d-31 mutant-expressing cells (Fig. 2f). The d-6 construct displayed a phenotype similar to FL, although the intracellular GFP signal was less prominent (Fig. 2c). Similar results were obtained in HeLa and 293 cells (data not shown). These data suggest that wild-type CXCR4 was trafficked to the plasma membrane but was internalized spontaneously. Thus, steady-state internalization appeared to be regulated by amino acids located between d-6 and d-10 (e.g. amino acids 343–346).

Steady-state and SDF-1α-induced CXCR4 internalization is genetically separable. Next, we investigated distribution of CXCR4 protein and cell migration after SDF-1α treatment. Confocal analysis showed that after SDF-1α exposure, cells expressing FL, d-6 and d-17 mutants showed GFP signals in intracellular compartments, which were enhanced 60 min after SDF-1α treatment, an effect most clearly shown in d-17-expressing cells (Fig. 3a). GFP signals from intracellular vesicles gradually disappeared 1–2 h after exposure to ligand. Such redistribution of GFP signals was not observed in cells expressing d-10, d-14, d-22, d-31 and d-44 (data not shown). Cell surface levels of CXCR4 before and after SDF-1α treatment were measured by FACS analysis undertaken with an antibody directed against the CXCR4 N-terminus, because that antibody did not interfere with ligand–receptor interaction (Fig. 3b). The downregulation of cell surface levels of FL 2 h after ligand exposure was 67.1 ± 11.1%, whereas that of d-44 was 96.3 ± 12.3% (average and standard deviation from 12 and 10 independent experiments, respectively), consistent with previous reports.[17,27,28] Ligand-induced downregulation of d-6 was 74.9 ± 12.9% ($n = 8$), similar to FL levels. Ligand-induced internalization was significantly less efficient in cells expressing d-10, d-14, d-17, d-22, d-31 and d-44 mutants when compared with FL ($P < 0.001$). Although the d-17 mutant supported ligand-facilitated internalization, as evidenced by microscopic observation, cell surface levels remained unchanged (Fig. 3a,b). This may be due in part to rapid recruitment of newly synthesized d-17 to the cell surface.

Next, we examined cells expressing CXCR4 mutants in response to SDF-1α. Migration results from intracellular signaling initiated by SDF-1α/CXCR4 interaction. Induction of cell migration by SDF-1α in cells expressing FL was 7.2-fold that of untreated cells ($P < 0.05$). In contrast, migration of cells expressing d-44 in response to SDF-1α was undetectable. These data are in agreement with a previous report.[26] The d-6 mutant, which is internalized upon SDF-1α treatment, supported ligand-promoted cell migration by 6.1-fold ($P < 0.01$) relative to untreated cells, similar to FL. Other deletion mutants tested did not display enhanced cell migration following ligand treatment, except for d-17, which showed modestly enhanced (1.9-fold) migration relative to untreated cells, which was not statistically significant. When basal migratory activities were compared, removal of six or more amino acids from the cytoplasmic tail appeared to potentiate migration in the absence of ligand (open bars, Fig. 3c). These data suggest that constitutive internalization is regulated independently of ligand-facilitated internalization.

Identification of CXCR4 S(E/D)S as a ligand-independent internalization motif. The above data indicated that the carboxy-terminal four

doi: 10.1111/j.1349-7006.2007.00388.x

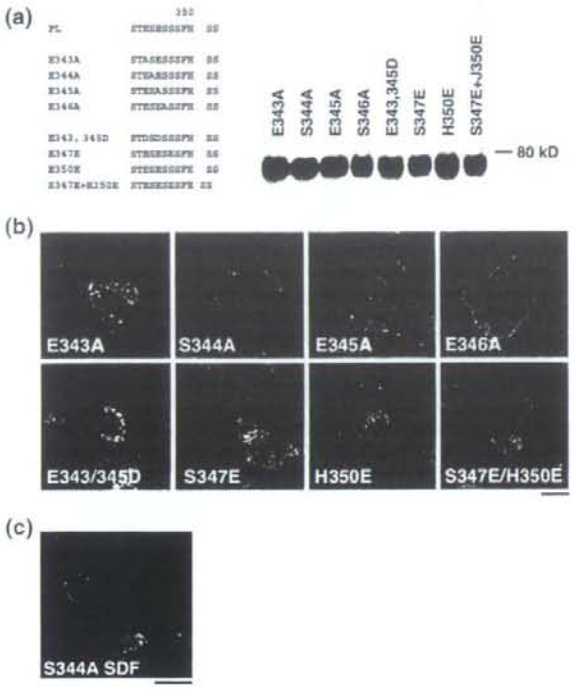

Fig. 4. Characterization of the SDF-1α-independent internalization motif of CXCR4. (a) Left, amino acid sequences of CXCR4 FL and substitution mutants. Letters in red indicate introduced mutations. Right, protein expression of each mutant in 293T cells was verified by Western blot analysis. (b) Confocal micrographs of NP2 cells expressing each mutant. The blue signal represents the Hoechst-stained nucleus. (Original magnification, ×630; bar, 10 μm.) (c) NP2 cells expressing the S344A mutant treated with SDF-1α for 2 h are shown. The blue signal represents the Hoechst-stained nucleus. (Original magnification, ×630; bar, 10 μm.)

amino acids (ESES; residues 343–346) likely function in ligand-independent CXCR4 internalization. To further characterize which amino acids are required for ligand-independent internalization, we generated alanine substitution mutants for each of the four amino acids in the context of FL and examined their phenotypes (Fig. 4a). Protein expression of mutants was verified in Western blot analysis (Fig. 4a). Among the four mutants, the E343A mutant showed the FL phenotype, while the others displayed the d-44 phenotype in the absence of ligand (Fig. 4b). These data demonstrate that Ser^{344}-Glu^{345}-Ser^{346} constitute the core motif for SDF-1α-independent CXCR4 internalization. Both E345A and S346A mutants exhibited the Thr^{342}-Glu^{343}-Ser^{344} sequence adjacent to the original SES sequence. However, this 'SES-like' motif did not support constitutive internalization, suggesting that Thr cannot substitute for Ser to maintain functionality as a constitutive internalization motif. We reasoned that if such a motif requires an acidic amino acid between two serine residues, changing Glu to Asp should maintain the motif's function. Thus, we constructed a mutant in which Glu was replaced with Asp (E343/345D; Fig. 4a). Also, to determine whether two adjacent SES sequences could augment the FL phenotype, we substituted Ser^{347} with Glu (S347E), creating an additional SES motif next to the original SES one (Fig. 4a). As controls, we created H350E and S347E/H350E mutants (Fig. 4a). Expression of these mutants was verified by Western blot analysis (Fig. 4a). Interestingly, the E343/345D mutant retained the FL phenotype (Fig. 4b), indicating that an acidic residue is required to maintain function of the constitutive internalization motif. S347E showed an intermediate phenotype in which numerous fine GFP-positive vesicles were seen close to the nucleus (Fig. 4b). These data indicate that the two adjacent SES sequences do not augment the FL phenotype but actually interfere with steady-state internalization. Both H350E and S347E/H350E mutants also showed an intermediate phenotype (Fig. 4b), suggesting that more than three acidic amino acids close to the SES motif may inhibit its function, potentially by generating a negative charge cluster. Overall, we conclude that the SDF-1α-independent internalization motif is located at amino acids 344–346 of the CXCR4 cytoplasmic tail.

Finally, we analyzed phenotypes of the S344A mutant in greater detail. Two hours after SDF-1α treatment, cells expressing this mutant showed accumulation of GFP signals at perinuclear regions, similar to the d-17 mutant (Figs. 1a and 4c). FACS analysis revealed that cell surface levels of S344A decreased to $70.8 \pm 11.7\%$ ($n = 7$) following SDF-1α treatment relative to untreated cells, almost as efficient as FL (Fig. 3b). Migratory activity of cells expressing the S344A mutant was stimulated 3.0-fold by SDF-1α, while that of cells expressing FL assayed in parallel showed a 5.8-fold increase relative to untreated cells. These data demonstrate that the S344A mutant, which is defective in constitutive internalization, can undergo ligand-dependent internalization and stimulate migration. Along with the d-17 data, our observations strongly suggest that genetic elements required for the ligand-dependent and -independent internalization are separable.

Discussion

We demonstrated here that CXCR4 is constitutively internalized in the absence of SDF-1α and that steady-state trafficking of CXCR4 is regulated by its cytoplasmic tail. We show that the three amino acid motif, Ser^{344}-Glu^{345}-Ser^{346}, within the cytoplasmic tail is essential for efficient steady-state internalization of CXCR4. Our work indicates that ligand-independent internalization of CXCR4 is genetically separable from ligand-dependent internalization: mutants defective in steady-state internalization (d-17 and S344A) were competent to respond to SDF-1α-promoted internalization signals. That residues required for ligand-dependent endocytosis (Ser324, 325, 330, 338, 339, Ile^{328} Leu^{329} and Lys^{331}; summarized in Fig. 1a)[16–18] do not overlap with those required for ligand-independent internalization, further supports the idea that these activities are separable.

Interestingly, the d-17 mutant displayed SDF-1α-promoted internalization, whereas the d-14 and d-22 mutants did not. These data suggest that an element between amino acids 336 and 342 negatively regulates ligand-initiated CXCR4 internalization. We are currently determining what amino acids are required for that motif. What is unique about the constitutive internalization motif is its position effect in terms of the distance of the motif from the "body" of the receptor. SES-like motifs can be found in the cytoplasmic tails of both CXC-chemokine receptors (for example, CXCR3) and CC-chemokine receptors including CCR2, CCR5 and CCR7. Indeed, these receptors share similar amino acid sequences in which two acidic amino acids (mostly Asp) positioned between the 36th and 45th amino acids of the cytoplasmic tail, where Ser and Thr residues are often in the close proximity to the acidic amino acids but positively charged amino acids, are infrequent. We hypothesize that for the ligand-independent internalization motif to function, the SES motif or its equivalent must be positioned at approximately the 40th residue of the cytoplasmic tail.

Many GPCR, including α1a-adrenoceptor, and the μ-opioid receptor, are spontaneously internalized.[36,37] Therefore, we conclude that various GPCR actively and continuously undergo endocytosis in the absence of ligand in a manner similar to

CXCR4 and hypothesize that the function of constitutive receptor internalization is to fine-tune the threshold at which cells sense ligand. Cells should be able to rapidly post up- and downregulate cell surface levels of CXCR4 using post-translational mechanisms. Such regulation should enable cells to migrate toward SDF-1α-rich tissues as needed and should also prevent inappropriate cells from migrating.

Our work is relevant to cancer cell metastasis and the pathogenesis of WHIM syndrome. Cell surface levels of CXCR4 positively correlate with cancer cells' ability to metastasize.[5,19] We hypothesize that enhanced metastatic capabilities of cancer cells could be due in part to mutations that disrupt the function of SES motif, which would result in upregulation of cell surface levels of signal-competent CXCR4 (as exemplified by the E344A mutant). As for WHIM syndrome, it was recently reported that it is due to mutations within CXCR4's cytoplasmic domain.[14,38] Interestingly, these mutations result in loss of SES motif. We predict that loss of the SES motif should increase cell surface CXCR4 levels. Although CXCR4 mutations generated here are not identical to reported WHIM mutations, the d-10 mutant resembles mutations seen in WHIM syndrome, and it exhibits enhanced basal cell migratory activity. Increased cell surface CXCR4 or increased migratory potential may contribute to WHIM pathogenesis. The response of d-10-expressing cells to SDF-1α, however, was not as robust as that of cells derived from WHIM.[39,40] This discordance may be partly due to the cell type differences, as we have employed a glioblastoma cell line for our studies.

Thus, CXCR4 is a potentially important therapeutic target not only for cancers but for other conditions such as HIV-1 infection, chronic autoimmune disease, and genetic disorders including WHIM syndrome. CXCR4 also plays critical roles in embryogenesis, homeostasis and inflammation. Although there are potential caveats for treating cancer with CXCR4 antagonists, our data furthers the understanding of mechanisms regulating CXCR4 and could be useful in devising therapeutic strategies.

Acknowledgments

We thank Drs Toshitada Takemori and Tsutomu Murakami for critical reading of the manuscript. This work was supported in part by the Japan Human Science Foundation, the Japanese Ministry of Health, Labor and Welfare, and the Japanese Ministry of Education, Culture, Sports, Science and Technology.

References

1 Gether U. Uncovering molecular mechanisms involved in activation of G protein-coupled receptors. *Endocr Rev* 2000; **21**: 90–113.
2 Ferguson SS. Evolving concepts in G protein-coupled receptor endocytosis: the role in receptor desensitization and signaling. *Pharmacol Rev* 2001; **53**: 1–24.
3 Sapede D, Rossel M, Dambly-Chaudiere C, Ghysen A. Role of SDF1 chemokine in the development of lateral line efferent and facial motor neurons. *Proc Natl Acad Sci USA* 2005; **102**: 1714–8. Epub 2005 January 19.
4 Coughlan CM, McManus CM *et al.* Expression of multiple functional chemokine receptors and monocyte chemoattractant protein-1 in human neurons. *Neuroscience* 2000; **97**: 591–600.
5 Muller A, Homey B, Soto H *et al.* Involvement of chemokine receptors in breast cancer metastasis. *Nature* 2001; **410**: 50–6.
6 Zou YR, Kottmann AH, Kuroda M, Taniuchi I, Littman DR. Function of the chemokine receptor CXCR4 in haematopoiesis and in cerebellar development. *Nature* 1998; **393**: 595–9.
7 Ma Q, Jones D, Borghesani PR *et al.* Impaired B-lymphopoiesis, myelopoiesis, and derailed cerebellar neuron migration in CXCR4- and SDF-1-deficient mice. *Proc Natl Acad Sci USA* 1998; **95**: 9448–53.
8 Wang JF, Park IW, Groopman JE. Stromal cell-derived factor-1alpha stimulates tyrosine phosphorylation of multiple focal adhesion proteins and induces migration of hematopoietic progenitor cells: roles of phosphoinositide-3 kinase and protein kinase C. *Blood* 2000; **95**: 2505–13.
9 Kawahata K, Ujikawa M, Egawa T *et al.* A cell-autonomous requirement for CXCR4 in long-term lymphoid and myeloid reconstitution. *Proc Natl Acad Sci USA* 1999; **96**: 5663–7.
10 Peled A, Petit I, Kollet O *et al.* Dependence of human stem cell engraftment and repopulation of NOD/SCID mice on CXCR4. *Science* 1999; **283**: 845–8.
11 Zeelenberg IS, Ruuls-Van Stalle L, Roos E. The chemokine receptor CXCR4 is required for outgrowth of colon carcinoma micrometastases. *Cancer Res* 2003; **63**: 3833–9.
12 Phillips RJ, Burdick MD, Lutz M, Belperio JA, Keane MP, Strieter RM. The stromal derived factor-1/CXCL12-CXC chemokine receptor 4 biological axis in non-small cell lung cancer metastases. *Am J Respir Crit Care Med* 2003; **167**: 1676–86.
13 Taichman RS, Cooper C, Keller ET, Pienta KJ, Taichman NS, McCauley LK. Use of the stromal cell-derived factor-1/CXCR4 pathway in prostate cancer metastasis to bone. *Cancer Res* 2002; **62**: 1832–7.
14 Hernandez PA, Gorlin RJ, Lukens JN *et al.* Mutations in the chemokine receptor gene CXCR4 are associated with WHIM syndrome, a combined immunodeficiency disease. *Nat Genet* 2003; **34**: 70–4.
15 Lefkowitz RJ, Shenoy SK. Transduction of receptor signals by beta-arrestins. *Science* 2005; **308**: 512–7.
16 Marchese A, Benovic JL. Agonist-promoted ubiquitination of the G protein-coupled receptor CXCR4 mediates lysosomal sorting. *J Biol Chem* 2001; **276**: 45 509–12.
17 Orsini MJ, Parent JL, Mundell SJ, Benovic JL, Marchese A. Trafficking of the HIV coreceptor CXCR4. Role of arrestins and identification of residues in the c-terminal tail that mediate receptor internalization. *J Biol Chem* 1999; **274**: 31 076–86.
18 Marchese A, Raiborg C, Santini F, Keen JH, Stenmark H, Benovic JL. The E3 ubiquitin ligase AIP4 mediates ubiquitination and sorting of the G protein-coupled receptor CXCR4. *Dev Cell* 2003; **5**: 709–22.
19 Darash-Yahana M, Pikarsky E, Abramovitch R *et al.* Role of high expression levels of CXCR4 in tumor growth, vascularization, and metastasis. *FASEB* 2004; **J 18**: 1240–2.
20 Vila-Coro AJ, Rodriguez-Frade JM, Martin De Ana A, Moreno-Ortiz MC, Martinez AC, Mellado M. The chemokine SDF-1alpha triggers CXCR4 receptor dimerization and activates the JAK/STAT pathway. *FASEB J* 1999; **13**: 1699–710.
21 Babcock GJ, Farzan M, Sodroski J. Ligand-independent dimerization of CXCR4, a principal HIV-1 coreceptor. *J Biol Chem* 2003; **278**: 3378–85.
22 Terrillon S, Bouvier M. Roles of G-protein-coupled receptor dimerization. *EMBO Rep* 2004; **5**: 30–4.
23 Hu H, Shioda T, Hori T *et al.* Dissociation of ligand-induced internalization of CXCR-4 from its co-receptor activity for HIV-1 Env-mediated membrane fusion. *Arch Virol* 1998; **143**: 851–61.
24 Yanagida M, Hayano T, Yamauchi Y *et al.* Human fibrillarin forms a sub-complex with splicing factor 2-associated p32, protein arginine methyltransferases, and tubulins alpha 3 and beta 1 that is independent of its association with preribosomal ribonucleoprotein complexes. *J Biol Chem* 2004; **279**: 1607–14.
25 Komano J, Miyauchi K, Matsuda Z, Yamamoto N. Inhibiting the Arp2/3 complex limits infection of both intracellular mature vaccinia virus and primate lentiviruses. *Mol Biol Cell* 2004; **15**: 5197–207.
26 Roland J, Murphy BJ, Ahr B *et al.* Role of the intracellular domains of CXCR4 in SDF-1-mediated signaling. *Blood* 2003; **101**: 399–406.
27 Haribabu B, Richardson RM, Fisher I *et al.* Regulation of human chemokine receptors CXCR4. Role of phosphorylation in desensitization and internalization. *J Biol Chem* 1997; **272**: 28 726–31.
28 Tarasova NI, Stauber RH, Michejda CJ. Spontaneous and ligand-induced trafficking of CXC-chemokine receptor 4. *J Biol Chem* 1998; **273**: 15 883–6.
29 Soda Y, Shimizu N, Jinno A *et al.* Establishment of a new system for determination of coreceptor usages of HIV based on the human glioma NP-2 cell line. *Biochem Biophys Res Commun* 1999; **258**: 313–21.
30 Zhang Y, Foudi A, Geay JF *et al.* Intracellular localization and constitutive endocytosis of CXCR4 in human CD34+ hematopoietic progenitor cells. *Stem Cells* 2004; **22**: 1015–29.
31 Mundy DI, Machleidt T, Ying YS, Anderson RG, Bloom GS. Dual control of caveolar membrane traffic by microtubules and the actin cytoskeleton. *J Cell Sci* 2002; **115**: 4327–39.
32 Rappoport JZ, Taha BW, Lemeer S, Benmerah A, Simon SM. The AP-2 complex is excluded from the dynamic population of plasma membrane-associated clathrin. *J Biol Chem* 2003; **278**: 47 357–60.
33 Rappoport JZ, Simon SM. Real-time analysis of clathrin-mediated endocytosis during cell migration. *J Cell Sci* 2003; **116**: 847–55.
34 Keyel PA, Watkins SC, Traub LM. Endocytic adaptor molecules reveal an endosomal population of clathrin by total internal reflection fluorescence microscopy. *J Biol Chem* 2004; **279**: 13 190–204.
35 Yarar D, Waterman-Storer CM, Schmid SL. A dynamic actin cytoskeleton functions at multiple stages of clathrin-mediated endocytosis. *Mol Biol Cell* 2005; **16**: 964–75.

doi: 10.1111/j.1349-7006.2007.00388.x

36 Pediani JD, Colston JF, Caldwell D, Milligan G, Daly CJ, McGrath JC. Beta-arrestin-dependent spontaneous alpha1a-adrenoceptor endocytosis causes intracellular transportation of alpha-blockers via recycling compartments. *Mol Pharmacol* 2005; **67**: 992–1004.
37 Segredo V, Burford NT, Lameh J, Sadee W. A constitutively internalizing and recycling mutant of the mu-opioid receptor. *J Neurochem* 1997; **68**: 2395–404.
38 Gulino AV, Moratto D, Sozzani S *et al.* Altered leukocyte response to CXCL12 in patients with warts hypogammaglobulinemia, infections, myelokathexis (WHIM) syndrome. *Blood* 2004; **104**: 444–52.
39 Kawai T, Choi U, Whiting-Theobald NL *et al.* Enhanced function with decreased internalization of carboxy-terminus truncated CXCR4 responsible for WHIM syndrome. *Exp Hematol* 2005; **33**: 460–8.
40 Balabanian K, Lagane B, Pablos JL *et al.* WHIM syndromes with different genetic anomalies are accounted for by impaired CXCR4 desensitization to CXCL12. *Blood* 2005; **105**: 2449–57.

Buoyant density and sedimentation dynamics of HIV-1 in two density-gradient media for semen processing

Naoaki Kuji, M.D., Ph.D.,[a] *Tsuyoshi Yoshii, M.D., Ph.D.,*[a] *Toshio Hamatani, M.D., Ph.D.,*[a] *Hideji Hanabusa, M.D., Ph.D.,*[c] *Yasunori Yoshimura, M.D., Ph.D.,*[a] *and Shingo Kato, Ph.D.*[b]

[a] Department of Obstetrics and Gynecology and [b] Department of Microbiology and Immunology, Keio University School of Medicine; and [c] Department of Hematology, Ogikubo Hospital, Tokyo, Japan

Objective: To compare buoyant density and sedimentation kinetics of human immunodeficiency virus 1 (HIV-1) in two sperm-washing media, Percoll and Pureception.
Design: Laboratory study.
Setting: University hospital.
Patient(s): None.
Intervention(s): Buoyant density and sedimentation kinetics of HIV-1 particles (MOLT-4/LAI strain) were measured in Percoll and Pureception using isopyknic ultracentrifugation and continuous-density-gradient centrifugation.
Main Outcome Measure(s): The HIV-1 particles were detected and semiquantified using a reverse transcription polymerase chain reaction (RT-PCR) for HIV-1 RNA.
Result(s): Calculated buoyant density of HIV-1 was approximately 1.042 in both media in isopyknic centrifugation. However, most HIV-1 particles were found in fractions with specific gravity less than 1.04 in both media, even after 40 minutes of density-gradient centrifugation at 1,600 *g*. Small viral accumulations were observed at the bottom of the tube in Pureception density gradients.
Conclusion(s): Although we found very high efficiency of HIV-1 removal using density-gradient centrifugation, a minute quantity of virus was found at the bottom of the gradient tube when Pureception was used as the medium. (Fertil Steril® 2008;■:■–■. ©2008 by American Society for Reproductive Medicine.)

Key Words: Sperm, Percoll, Pureception, density-gradient centrifugation, HIV-1, isopyknic centrifugation

Transmission of human immunodeficiency virus type 1 (HIV-1) through semen is widely recognized. Many studies have demonstrated that HIV-1 exists both as free virus in the seminal plasma and as cell-associated virus in semen (1–8). Sperm preparation techniques originally developed to separate the fraction containing highly motile spermatozoa from that of seminal plasma and nonmotile cells have been reported to reduce HIV-1 RNA and proviral DNA to undetectable concentrations (9, 10).

Increasingly, serodiscordant couples with an HIV-1–positive husband and an HIV-1–negative wife are requesting insemination techniques for avoiding risk of transmission to the female partner and to offspring (11). Intrauterine insemination (IUI), in vitro fertilization (IVF), and intracytoplasmic sperm injection (ICSI) after sperm preparation by techniques commonly referred to as "sperm washing" have been suggested as ways to reduce likelihood of transmission of HIV-1. Numerous pregnancy successes without HIV-1 seroconversions have been reported (12–14).

Sperm washing as the first step of the virus elimination procedure has used density-gradient centrifugation. Because HIV-1 infection is believed to worsen the condition of sperm, men with chronic HIV-1 infection often have abnormal semen profiles (15). An optimal washing method would maximize recovery of spermatozoa without decreasing viral removal efficacy. To the best of our knowledge, however, precise reliable data have not been obtained concerning buoyant density or sedimentation kinetics of HIV-1 in density-gradient media such as polyvinylpyrrolidone (PVP)-coated colloid-silica gel (Percoll) or silane-coated colloid-silica gel (Pureception). The latter medium has been used increasingly in place of Percoll.

In the present study, we determined the buoyant density of free HIV-1 in each of two sperm-washing media, Percoll and Pureception, using a highly sensitive nested competitive reverse transcription polymerase chain reaction (RT-PCR) technique that we established previously (10). Sedimentation dynamics in continuous density gradients using these two media also were investigated.

Received May 30, 2007; revised and accepted September 13, 2007.
Supported in part by a Grant-in-Aid for Scientific Research from the Ministry of Education, Science and Culture of Japan (no. 12671629).
Reprint requests: Naoaki Kuji, M.D., Ph.D., Department of Obstetrics and Gynecology, School of Medicine, Keio University, 35 Shinanomachi, Shinjuku-ku, Tokyo 160-8582, Japan (FAX: +81-3-3226-1667; E-mail: naoaki@sc.itc.keio.ac.jp).

0015-0282/08/$34.00
doi:10.1016/j.fertnstert.2007.09.025

MATERIALS AND METHODS

Reagents

Each concentration of Pureception solution was prepared by diluting 90% Pureception with sperm-washing medium (both from Sage In Vitro Fertilization, Pasadena, CA). Each concentration of Percoll solution was prepared by diluting 80% Percoll according to the method of Kaneko et al. (16), using 10 mmol/L HEPES-buffered Hanks solution (pH 7.4) including 4.0 mg/mL human serum albumin and antibiotics (0.14 mg/mL latamoxef sodium and 0.11 mg/mL ampicillin).

Viral RNA Quantification

A concentrated suspension of wild-type HIV-1 LAI strain produced from chronically infected MOLT-4 cells was used as the source of virus (10). As a quantification method for HIV-1, we used a nested competitive RT-PCR technique that we developed previously (10). Briefly, the internal competitor DNA consisted of an HIV-1 *env* sequence (nucleotide positions 6201 to 8805 according to NL4–3) (17) with deletion of positions 7119 to 7241 and addition of a T7 promoter (TAA TAC GAC TCA CTA TAG GGA GA) at the 5′ terminus. Internal competitor RNA was synthesized from the competitor DNA with T7 RNA polymerase. The DNA and RNA were quantified by spectrophotometry and end point dilution followed by Poisson analysis of positive scores from nested PCR, as described previously. Using this method, viral load has been confirmed to be maintained consistently at approximately 10 copies/20 μL.

Determination of Buoyant Density of HIV-1 by Isopyknic Focusing

The HIV-1 LAI strain (0.2 mL) was mixed with 2.5 mL 65% Percoll or 2.5 mL 50% Pureception (final viral concentration 1.15×10^6/mL). After centrifugation at 16,400 *g* (Percoll) or 11,400 *g* (Pureception) for 20 minutes, aliquots of the postcentrifugation suspension (each approximately 0.25 mL) were fractionated beginning at the bottom of the tube. Mean specific gravity of each fraction was determined by weighing 100 μL of each solution using a measuring micropipette. Viral concentration was determined by nested competitive RT-PCR, and p24 antigen was quantified with MiniVidas (Biomerieux, Marcy l'Etoile, France). Buoyant density of HIV-1 particles was determined from the solvent density corresponding to a peak of viral distribution.

Preparation of Continuous Density Gradients with a Gradient Pump and Evaluation of Sedimentation Dynamics

Two pairs of solutions as described subsequently were mixed in a pump for column preparation (Bio-Rad, Philadelphia, PA) to prepare 3-mL continuous density gradients: either a mixture of 80% Percoll and Hanks solution or a mixture of 90% Pureception and sperm-washing medium. A 0.2-mL aliquot of the concentrated HIV-1 suspension was layered on top of the upper layer of the prepared density gradient. After centrifugation at 1,600 *g* for 5, 10, 20, and 40 minutes, aliquots of the postcentrifugation suspension (approximately 0.25 mL) were fractionated beginning at the bottom of the tube. Mean specific gravity was determined, and viral load in each fraction was quantified using the nested competitive RT-PCR technique.

FIGURE 1

Viral RNA load in each density fraction of Percoll. Fractions were collected from the bottom and analyzed for density, human immunodeficiency virus 1 (HIV-1) RNA (*squares*), and p24 (*circles*). The HIV-1 RNA and p24 amounts were plotted against the density of each fraction, using a semilogarithmic scale. Both HIV-1 RNA and p24 showed a single peak at the position representing a density of 1.042.

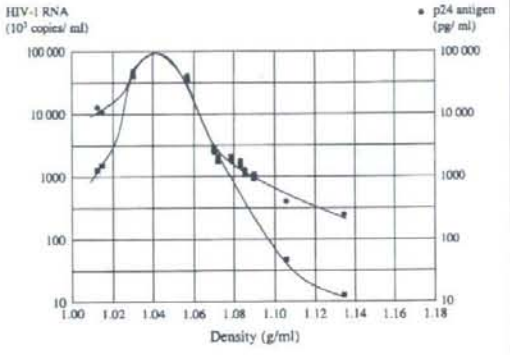

Kuji. Sedimentation kinetics of HIV-1. Fertil Steril 2008.

RESULTS

Buoyant Density in Percoll and Pureception

Viral RNA amounts, p24 antigen amounts, and medium density were determined in each of 12 fractions of a centrifuged mixture of HIV-1 LAI strain and 65% Percoll. Viral RNA and p24 antigen amounts were plotted against measured medium density using a semilogarithmic scale (Fig. 1). Assuming viral distribution curves to be normally distributed, distribution peaks of HIV-1 RNA and p24 antigen were calculated to exist at approximately 1.042 g/mL. Accordingly, the buoyant density of HIV-1 in Percoll was estimated to be 1.042 g/cm^3. Data for Pureception are presented in Figure 2. The buoyant density of HIV-1 in Pureception was estimated to be 1.042 g/cm^3, the same value as with Percoll. Viral distribution had a single peak in Percoll but showed two peaks in Pureception, with a small amount of virus in the higher-density fraction (bottom of the tube) in addition to the main peak.

Sedimentation Dynamics in Percoll and Pureception

High reproducibility was observed in the two continuous density gradients ranging from 0% to 90% Pureception and 0% to 80% Percoll. Linearity was maintained even after centrifugation at 1,600 *g* for 40 minutes (data not shown).

FIGURE 2

Viral RNA load in each density fraction of Pureception. Fractions were collected from the bottom and analyzed for density, human immunodeficiency virus 1 (HIV-1) RNA (*squares*), and p24 (*circles*). The HIV-1 RNA and p24 amounts were plotted against the density of each fraction, using a semilogarithmic scale. Amounts of p24 showed a single peak as for Percoll. The HIV-1 RNA amounts, however, showed two peaks: a small amount of virus at the higher-density position (the bottom of the centrifugation tube) in addition to the main peak.

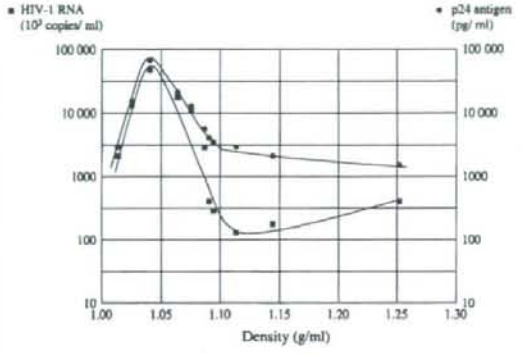

Kuji. Sedimentation kinetics of HIV-1. Fertil Steril 2008.

FIGURE 3

The human immunodeficiency virus 1 (HIV-1) viral load after centrifugation in Percoll and in Pureception (1,600 *g*). Concentrated HIV-1 suspension was layered on top of either Percoll or Pureception density gradient and centrifuged at 1,600 *g* for 5, 10, 20, or 40 minutes. Beginning at the bottom of the tube, each 0.25-mL aliquot was removed as a fraction and then analyzed. Viral load after centrifugation for 10 minutes (*sold squares:* Percoll; *open squares:* Pureception), and 40 minutes (*solid circles:* Percoll; *open circles:* Pureception) are shown. Most HIV-1 particles were present in fractions with specific gravity near or below 1.04, even after 40 minutes of centrifugation in continuous density gradients using both Percoll and Pureception. With Pureception, however, small viral accumulations were observed at the bottom of the tube (data not shown), a finding absent with Percoll.

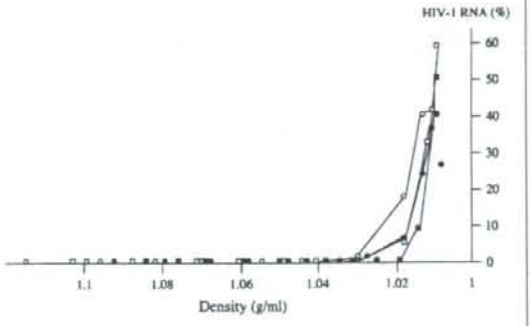

Kuji. Sedimentation kinetics of HIV-1. Fertil Steril 2008.

Using the continuous density gradients described, sedimentation dynamics of HIV-1 layered on the top of the upper layer of each gradient were investigated. Most HIV-1 particles were found in fractions with specific gravity less than 1.04, even after 40 minutes of centrifugation, in both continuous density gradient media (Fig. 3). In Pureception, however, small viral accumulations were observed at the bottom of the tube (data not shown), a finding absent with Percoll.

DISCUSSION

When the male partner is HIV-1 positive, a female partner who is HIV-1 negative is estimated to incur a 0.1% to 0.2% risk of acquiring HIV-1 per act of unprotected intercourse (18). Thus, attempting to conceive naturally carries a serious risk to the uninfected female partner and to the child (19). Density-gradient centrifugation techniques can effectively eliminate HIV-1 from semen to reduce the risk of HIV-1 transmission in HIV-1–discordant couples wishing to have children (9, 10). Although Baccetti et al. (3) detected HIV-1 particles and HIV-1 nucleic acid in ejaculated washed sperm preparations from HIV-1–seropositive patients, other investigators noted total absence of HIV-1 particles and nucleic acid in washed sperm (1, 7, 20). Thus, separation of seminal fluid and cellular elements from sperm by washing techniques reduces the viral load of semen detected by PCR and RT-PCR. Consequently, several groups have achieved pregnancy successes without HIV-1 seroconversions by using sperm-washing methods (12, 13).

Separation of spermatozoa using density-gradient centrifugation is possible in part because spermatozoa are motile, unlike other particulates present; additionally, sedimentation velocities differ between spermatozoa, seminal plasma, lymphocytes, and free virus. Highly motile spermatozoa migrate more quickly than nonmotile constituents during density-gradient centrifugation, because centrifugal force orients them with head downward and tail upward (21). Because motility thus contributes importantly to separation, efficiency ordinarily is enhanced for spermatozoa owing to their motility. In contrast, for spermatozoa with impaired motility, especially those from HIV-1–positive men with infertility from factors such as oligozoospermia or asthenozoospermia, buoyant density as well as sedimentation velocity of the virus in sperm-washing media become the most important factors for separating virus from sperm. With poorly motile spermatozoa, density-gradient viral separation is likely to fail unless centrifugation-related factors are carefully considered.

In the present study, we investigated sedimentation dynamics of HIV-1 in two extensively used sperm-washing media, Percoll and Pureception. Percoll, a colloidal suspension of PVP-coated silica particles, has been used widely for sperm processing in assisted reproductive technology, offering simplicity, rapidity, and excellent yields. In 1996, however, Percoll was withdrawn from clinical use in humans because of concern over possible endotoxin contamination. Pureception, a colloidal suspension of silane-coated silica particles developed as a substitute, has been shown to be effective in recovering motile sperm by several studies comparing it with Percoll, and it is now used worldwide (22–26).

The buoyant density for HIV-1 in a linear sucrose gradient was reported to be 1.16 g/mL (27), which differs from the buoyant density of 1.04 g/mL obtained in the present experiment with both sperm-washing density gradient media, Percoll and Pureception. In isopyknic focusing, buoyant densities of particles can vary considerably according to the composition of the density gradient media used, reflecting differences in osmolarity of the medium (28). We therefore took care to use the same density gradient media actually used for sperm washing in determining the buoyant density of HIV-1. This value proved to be equal between the two sperm washing media, Percoll and Pureception, probably because both consist mainly of silica gel. Their osmotic pressures were kept equal in view of their having a common use, processing of spermatozoa.

We also examined the sedimentation velocity of HIV-1 in continuous density gradients made of Percoll and Pureception. These continuous-gradient columns, prepared with a gradient pump, demonstrated high reproducibility and post-centrifugation stability. In clinical settings, use of discontinuous density gradients is quite common, whereas continuous density gradients are rarely used, because highly specialized equipment and personnel are required to prepare reproducible gradients. However, with discontinuous density gradients, virus may be trapped at the interface between densities and the sedimentation rate of the virus also may change as a result of viral aggregation–especially when high concentrations of virus are applied, as in the present study. For that reason, we used continuous density gradients for determination of the distribution of viral particles among the sedimentation fractions. High concentrations of HIV-1 were layered on the upper surface of the continuous density gradient before centrifugation. Even after centrifugation at 1600 *g* for 40 minutes, almost all HIV-1 virus particles remained in the superficial fractions where density was near or less than 1.042, the determined buoyant density of HIV-1. This confirmed that the sedimentation velocity of HIV-1 was very low in continuous density gradients made up from either Percoll or Pureception.

Interestingly, minute amounts of virus were found to be clustered at the bottom of the Pureception gradient tube but not the Percoll gradient tube. The reason for this difference remains unknown, but one possible explanation might involve a difference in silica particle size between Percoll and Pureception. The average diameter of Percoll particles is about 17.2 nm, and the size of the particles in Pureception before silane coating is about 15 nm; the density-gradient particles in Percoll would appear to be slightly larger than those in Pureception. Another possible explanation might involve differences in the substances coating the silica particles. Silane (in Pureception) might exert slightly less friction against various particles than PVP (in Percoll). In fact, the recovery rate of spermatozoa has been reported to be greater using Pureception than using Percoll (22). The decreased friction in Pureception might permit small HIV-1 aggregates to form.

Effectiveness of clinical management of HIV-1–serodiscordant couples using sperm washing followed by a swim-up technique is presently under investigation. After carrying out artificial insemination in more than 300 cases, Semprini et al. (12) reported that transmission of infection was prevented successfully in all subjects. In contrast, another study found transmission of infection in some cases where the semen was subjected only to a washing procedure (29). Although several problems remain to be solved, the American Society for Reproductive Medicine recommended in 2004 that procedures for HIV-1–discordant couples wanting a child can be performed, but only at institutions able to provide the most effective methods of sperm preparation as well as the rigorous testing and treatment necessary to minimize the chance of HIV-1 transmission to partner and offspring (30).

In conclusion, we investigated the buoyant density of HIV-1 and dynamic changes in the sedimentation pattern of free HIV-1 in both Percoll and Pureception media for "sperm washing." We found very high efficiency of free virus removal using either medium for density-gradient centrifugation. However, a minute quantity of virus was found at the bottom of the gradient tube in addition to the virus retained in overlying fractions when Pureception was used as the medium. Accordingly, washing procedures used clinically must be assessed individually in terms of specific type of density gradient medium.

Acknowledgements: The authors acknowledge the assistance of Ms. Kazuyo Nakamura, B.A. in preparing the manuscript.

REFERENCES

1. Quayle AJ, Xu C, Mayer KH, Anderson DJ. T Lymphocytes and macrophages, but not motile spermatozoa, are a significant source of human immunodeficiency virus in semen. J Infect Dis 1997;176:960–8.
2. Baccetti B, Benedetto A, Burrini AG, Collodel G, Elia C, Piomboni P, et al. HIV particles detected in spermatozoa of patients with AIDS. J Submicrosc Cytol Pathol 1991;23:339–45.
3. Baccetti B, Benedetto A, Burrini AG, Collodel G, Ceccarini EC, Crisa N, et al. HIV-particles in spermatozoa of patients with AIDS and their transfer into the oocyte. J Cell Biol 1994;127:903–14.
4. Scofield VL, Rao B, Broder S, Kennedy C, Wallace M, Graham B, et al. HIV interaction with sperm. AIDS 1994;8:1733–6.
5. Bagasra O, Farzadegan H, Seshamma T, Oakes JW, Saah A, Pomerantz RJ. Detection of HIV-1 proviral DNA in sperm from HIV-1-infected men. AIDS 1994;8:1669–74.
6. Gobert B, Amiel C, Tang JQ, Barbarino P, Bene MC, Faure G. CD4-like molecules in human sperm. FEBS Lett 1990;261:339–42.

7. Lasheeb AS, King J, Ball JK, Curran R, Barratt CL, Afnan M, et al. Semen characteristics in HIV-1 positive men and the effect of semen washing. Genitourin Med 1997;73:303–5.
8. Nuovo GJ, Becker J, Burk MW, Margiotta M, Fuhrer J, Steigbigel RT. In situ detection of PCR-amplified HIV-1 nucleic acids in lymph nodes and peripheral blood in patients with asymptomatic HIV-1 infection and advanced-stage AIDS. J Acquir Immune Defic Syndr 1994;7:916–23.
9. Kim LU, Johnson MR, Barton S, Nelson MR, Sontag G, Smith JR, et al. Evaluation of sperm washing as a potential method of reducing HIV transmission in HIV-discordant couples wishing to have children. AIDS 1999;13:645–51.
10. Hanabusa H, Kuji N, Kato S, Tagami H, Kaneko S, Tanaka H, et al. An evaluation of semen processing methods for eliminating HIV-1. AIDS 2000;14:1611–6.
11. Semprini AE, Levi-Setti P, Bozzo M, Ravizza M, Taglioretti A, Sulpizio P, et al. Insemination of HIV-negative woman with processed semen of HIV-positive partners. Lancet 1992;340:1317–9.
12. Semprini AE, Fiore S, Pardi G. Reproductive counselling for HIV-discordant couples. Lancet 1997;349:1401–2.
13. Marina S, Marina F, Alcolea R, Exposito R, Huguet J, Nadal J, et al. Human immunodeficiency virus type 1-serodiscordant couples can bear healthy children after undergoing intrauterine insemination. Fertil Steril 1998;70:35–9.
14. Weigel MM, Gentili M, Beichert M, Friese K, Sonnenberg-Schwan U. Reproductive assistance to HIV-discordant couples—the German approach. Eur J Med Res 2001;6:259–62.
15. Pena JE, Thornton MH Jr, Sauer MV. Reversible azoospermia: anabolic steroids may profoundly affect human immunodeficiency virus-seropositive men undergoing assisted reproduction. Obstet Gynecol 2003;101:1073–5.
16. Kaneko S, Sato H, Kobanawa K, Oshio S, Kobayashi T, Iizuka R. Continuous-step density gradient centrifugation for the selective concentration of progressively motile sperm for insemination with husband's semen. Arch Androl 1987;19:75–84.
17. Adachi A, Gendelman HE, Koenig S, Folks T, Willey R, Rabson A, et al. Production of acquired immunodeficiency syndrome-associated retrovirus in human and nonhuman cells transfected with an infectious molecular clone. J Virol 1986;59:284–91.
18. Mastro TD, de Vincenzi I. Probabilities of sexual HIV-1 transmission. AIDS 1996;10(Suppl A):S75–82.
19. Mandelbrot L, Heard I, Henrion-Geant E, Henrion R. Natural conception in HIV-negative women with HIV-infected partners. Lancet 1997;349: 850–1.
20. Pudney J, Nguyen H, Xu C, Anderson DJ. Microscopic evidence against HIV-1 infection of germ cell or attachment to sperm. J Reprod Immunol 1999;44:57–77.
21. Gorus FK, Pipeleers DG. A rapid method for the fractionation of human spermatozoa according to their progressive motility. Fertil Steril 1981;35:662–5.
22. Perez SM, Chan PJ, Patton WC, King A. Silane-coated silica particle colloid processing of human sperm. J Assist Reprod Genet 1997;14: 388–93.
23. Claassens OE, Menkveld R, Harrison KL. Evaluation of three substitutes for Percoll in sperm isolation by density gradient centrifugation. Hum Reprod 1998;13:3139–43.
24. Chen MJ, Bongso A. Comparative evaluation of two density gradient preparations for sperm separation for medically assisted conception. Hum Reprod 1999;14:759–64.
25. Soderlund B, Lundin K. The use of silane-coated silica particles for density gradient centrifugation in in-vitro fertilization. Hum Reprod 2000;15:857–60.
26. Mousset-Simeon N, Rives N, Masse L, Chevallier F, Mace B. Comparison of six density gradient media for selection of cryopreserved donor spermatozoa. J Androl 2004;25:881–4.
27. Cimarelli A, Sandin S, Hoglund S, Luban J. Basic residues in human immunodeficiency virus type 1 nucleocapsid promote virion assembly via interaction with RNA. J Virol 2000;74:3046–57.
28. Pertoft H. Fractionation of cells and subcellular particles with Percoll. J Biochem Biophys Methods 2000;44:1–30.
29. Centers for Disease Control (CDC). Epidemiologic notes and reports: HIV-1 infection and artificial insemination with processed semen. MMWR Morb Mortal Wkly Rep 1990;249:255–6.
30. Ethics Committee of the American Society for Reproductive Medicine. Human immunodeficiency virus and infertility treatment. Fertil Steril 2004;82(suppl 1):S228–31.

ANTIMICROBIAL AGENTS AND CHEMOTHERAPY, Feb. 2008, p. 782–785
0066-4804/08/$08.00+0 doi:10.1128/AAC.01613-06

Vol. 52, No. 2

Intracellular Efavirenz Levels in Peripheral Blood Mononuclear Cells from Human Immunodeficiency Virus-Infected Individuals▽

Rie Tanaka,[1] Hideji Hanabusa,[2] Ei Kinai,[2] Naoki Hasegawa,[1] Masayoshi Negishi,[1] and Shingo Kato[1]*

Keio University School of Medicine[1] and Ogikubo Hospital,[2] Tokyo, Japan

Received 27 December 2006/Returned for modification 15 March 2007/Accepted 28 November 2007

We describe a novel method for isolating plasma-free peripheral blood mononuclear cells retaining intracellular efavirenz. Quantification of efavirenz in 13 human immunodeficiency virus-infected patients by liquid chromatography-tandem mass spectrometry showed a higher correlation of intracellular levels with unbound plasma levels (accumulation ratio, 1,190) than with total plasma levels.

Efavirenz, a nonnucleoside reverse transcriptase inhibitor, is a major component of current antiretroviral therapy for human immunodeficiency virus (HIV) type 1 infection. Several studies supported the idea of the usefulness of therapeutic drug monitoring of efavirenz, because viral suppression and adverse effects are associated with efavirenz levels in plasma (3, 9). Given that efavirenz exerts inhibitory activity with respect to reverse transcriptase and may interact with cellular enzymes within the cell, it is likely that intracellular levels are more relevant to the clinical outcome than plasma levels (10). Intracellular efavirenz levels have been explored using similar procedures, which consisted of preparation of peripheral blood mononuclear cells (PBMCs) by Ficoll density gradient centrifugation and cell washing with ice-cold phosphate buffered saline (PBS) (1, 2, 10). During our preliminary experiments, it was observed that efavirenz in PBS strongly stuck to the surface of plastic microcentrifuge tubes and was difficult to wash away with PBS. Such a property of adherence of efavirenz may have affected measurements of intracellular quantities in the previous protocols.

First, the efflux rate of efavirenz from cells was studied. PBMCs isolated from a healthy donor by use of Ficoll-Paque Plus solution (GE Healthcare, Piscataway, NJ) were incubated in 1 μM efavirenz in serum-free VP-SFM medium (Invitrogen, Carlsbad, CA) at 37°C for 1 h and then transferred to drug-free medium and incubated at either 4°C or 37°C for up to 20 min. Three aliquots of 10^6 cells were taken at each time point, and the efavirenz contained in each aliquot was extracted with 80% methanol and quantified by liquid chromatography-tandem mass spectrometry (LC-MS/MS) with a high-performance LC system (Agilent 1100 Series; Agilent, Palo Alto, CA) and a tandem mass spectrometer (API QStar Pulsar *I*; Applied Biosystems, Foster City, CA) using electrospray ionization in which an *m/z* transition of 333 to 272 atomic mass units for $(M+NH_4)^+$ precursor ions of efavirenz was used. As shown in Fig. 1, the intracellular efavirenz concentration declined within 5 min at either 37°C or 4°C to a level near the background level. This result poses another question about the previous isolation procedures used for PBMCs, because they were based on the assumption that drug efflux produced during washing procedure is suppressed by the use of ice-cold PBS. This result, taken together with those demonstrating the highly lipophilic property of efavirenz, suggests that intracellular efavirenz is eluted from the cells and adsorbed to the surface of plastic vessels during cell washing. To examine this hypothesis we compared quantifications of levels of efavirenz in PBMCs by two different isolation protocols: one used the same tube during washing, and the other used new tubes in each washing (Table 1). Transfer of cell suspension to a new tube each time reduced the efavirenz quantity remarkably compared with the use of the same tube throughout washing. These results suggest that the drug exudes from cells during cell washing and that the drug present in residual plasma was not washed away in studies employing the previously used procedures.

Thus, we decided to develop a new method for isolation of PBMCs (Fig. 2). The method consists of three steps: banding of PBMCs at the bottom of the plasma layer but not in the Ficoll-Paque solution by a relatively short centrifugation time; washing of PBMCs with concurrently prepared plasma of the same patient; and separation of PBMCs from the plasma by centrifugation through silicone oil (supplemented with 8% *n*-hexadecane) in a "double tube." By this method, efavirenz in PBMCs are kept equilibrated with the efavirenz in plasma until

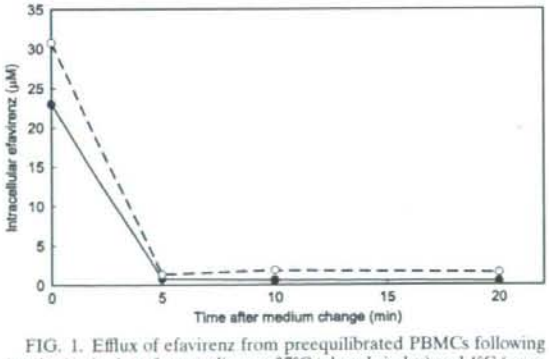

FIG. 1. Efflux of efavirenz from preequilibrated PBMCs following incubation in drug-free medium at 37°C (closed circles) and 4°C (open circles).

* Corresponding author. Mailing address: Department of Microbiology and Immunology, Keio University School of Medicine, 35 Shinanomachi, Shinjuku-ku, Tokyo 160-8582, Japan. Phone: 81 3 5363 3769. Fax: 81 3 5360 1508. E-mail: skato@sc.itc.keio.ac.jp.

▽ Published ahead of print on 10 December 2007.

TABLE 1. Quantification of efavirenz in PBMCs isolated by the present method and a previously reported method[a]

Source	Intracellular efavirenz concn[b] (μM)		
	Previous method with one tube[c]	Previous method with new tubes[d]	Present method[e]
Spiked donor blood[f]	110 ± 19	4.6 ± 1.7	97 ± 17
Patient 1	Not assayed	3.8 ± 1.3	63 ± 24
Patient 2	Not assayed	1.1 ± 0.3	71 ± 11

[a] The method reported by Almond et al. (1) was used for isolation of PBMCs for comparison with the present method.
[b] Efavirenz was quantified by LC-MS/MS. Intracellular concentrations were calculated, taking 0.25 pl as the volume of a single cell (5). Data are expressed as means ± standard deviations (n = 3).
[c] Washing of PBMCs in ice-cold PBS was carried out three times in the same microcentrifuge tube.
[d] Suspension of PBMCs in ice-cold PBS was transferred into a new microcentrifuge tube for centrifugation before each of three washings.
[e] Intracellular efavirenz concentrations were determined as described in the legend to Fig. 2.
[f] HIV-uninfected donor blood was spiked with efavirenz at 10 μM.

PBMCs are separated from the plasma. The use of a "double tube" in centrifugation prevents plasma from contaminating the surface of an outer microcentrifuge tube and thus from getting into the extract of PBMCs.

By using this method, we studied the dependence of intracellular efavirenz levels on the concentration of plasma in medium containing efavirenz at 10 μM. Efavirenz not bound by protein was obtained by use of a Centrifree micropartition device (Centrifree, Billerica, MA). The intracellular efavirenz concentration decreased with an increase in the plasma concentration (Fig. 3A) and was proportional to the unbound efavirenz concentration in medium, with a mean intracellular accumulation ratio of 970 (Fig. 3B). These results show that the major determinant of intercellular efavirenz levels is extracellular unbound levels but not total extracellular levels, which agrees with the pharmacological idea that only unbound drug is able to enter the cell.

Next, the relationships between total plasma, unbound plasma, and intracellular efavirenz concentrations were studied using samples from 13 patients receiving antiretroviral agents containing efavirenz in Keio University Hospital (Tokyo, Japan). The patients provided written informed consent for the study, which was approved by the local ethics committee. The median duration of treatment was 15 months, with a range from 1 to 65 months. Concurrent drugs used for treatment were zidovudine and lamivudine (3TC) for four patients, stavudine and 3TC for five, tenofovir disoproxil fumarate and emtricitabine for three, and tenofovir disoproxil fumarate and 3TC for one. All patients were Japanese males and exhibited no biochemical evidence of impairment of the liver or kidney. Although there were significant associations between total and unbound plasma levels (Spearman's rank correlation coefficient [rs] = 0.66; P = 0.021) (Fig. 4A) and between total plasma and intracellular levels (rs = 0.66; P = 0.021) (Fig. 4B), a stronger correlation was observed between unbound plasma and intracellular levels (rs = 0.76; P = 0.0082) (Fig. 4C), with a mean accumulation ratio of 1,190.

The results presented above are contrasted with the results

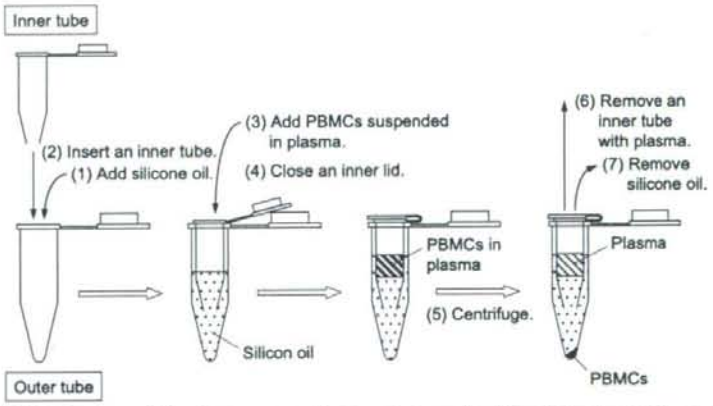

FIG. 2. Preparation of PBMCs for intracellular efavirenz quantification. Anticoagulated blood (1 ml) was layered on 800 μl of a Ficoll-Paque Plus solution (GE Healthcare, Piscataway, NJ) and centrifuged at 180 × g for 10 min. After centrifugation, PBMCs which formed a layer at the boundary between plasma and Ficoll-Paque Plus solution were collected and centrifuged at 320 × g for 2 min. Precipitated PBMCs were washed in 100 μl of plasma prepared from the same blood and centrifuged at 500 × g for 2 min. PBMCs were separated from plasma as follows: (i) a mixture of silicone oil (catalog no. SH-550; Nacalai, Kyoto, Japan) and n-hexadecane (Nakalai) (800 μl; 92:8 [vol/vol]) was added into an outer tube (1.5-ml microcentrifuge tube); (ii) an inner tube (made from a 0.5-ml microcentrifuge tube) with a hole at the bottom was sunk in silicone oil in the outer tube; (iii) PBMCs suspended in 100 μl of plasma were layered on silicone oil in the inner tube; (iv) the lid of the inner tube was pressed down; (v) an assembled "double tube" was centrifuged at 16,000 × g for 1 min, thereby precipitating PBMCs quickly to the bottom of the outer tube; (vi) the inner tube containing plasma and silicone oil was removed, with the lid kept closed to prevent plasma falling into the outer tube; and (vii) silicone oil was removed while leaving pelleted PBMCs in place and then the remaining silicone oil on the tube surface was removed after a brief centrifugation. Pelleted PBMCs were suspended in 30 μl of water, and immediately 10 μl of the suspension was used for determination of cell numbers with a cell counter (Celltac; Nihon Kohden, Tokyo, Japan); note that suspending cells in PBS is not recommended, because the presence of phosphate ions in samples affects ionization of molecules in mass spectrometry and sometimes causes severe troubles to the machine. To the remaining cell suspension, 80 μl of methanol was added, and efavirenz was quantified by LC-MS/MS.

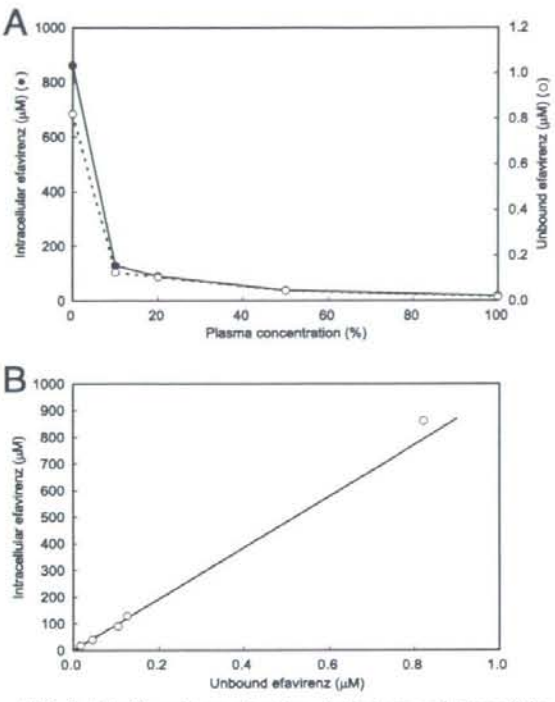

FIG. 3. (A) Dependence of unbound efavirenz and intracellular efavirenz levels on plasma content (expressed in percentages) in medium containing efavirenz at 10 μM. (B) Relationship between unbound and intracellular efavirenz concentrations as deduced from the data presented in panel A.

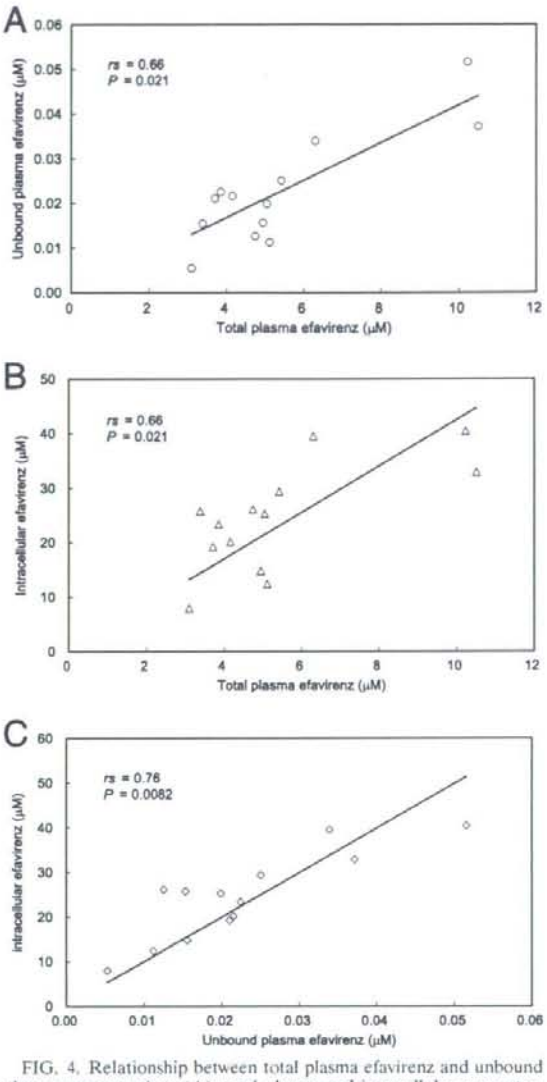

FIG. 4. Relationship between total plasma efavirenz and unbound plasma concentrations (A), total plasma and intracellular concentrations (B), and unbound plasma and intracellular concentrations (C) in samples from 13 patients receiving antiretroviral therapy that included efavirenz treatment. Data were analyzed by Spearman rank correlation.

of previous studies (1, 10) and demonstrate that intracellular efavirenz levels are not correlated with unbound plasma levels but are significantly correlated with total plasma levels. They indicate that total plasma efavirenz concentrations may be good surrogate markers for intracellular concentrations and that binding of efavirenz to plasma protein may be linked to its binding to unknown materials in cells. It should be noted that these studies used similar methods for isolation of PBMCs in which PBMC extract is, as argued above, apt to be contaminated with plasma efavirenz. If such contamination occurred in their studies, it would be inevitable that a stronger correlation would be observed between total plasma and intracellular efavirenz levels.

Efavirenz was highly accumulated in resting PBMCs. This may have been due to the binding to cellular protein or membrane because of its high lipophilicity ($\log_P$ = 5.4). Efavirenz bound to cellular components is unlikely to play a direct role in inhibition of reverse transcriptase activity. To study further the biological significance of intracellular drugs, new technologies for quantifying intracellular unbound drug and for identifying intracellular drug localization are required.

Most protease inhibitors also have the properties of rapid excretion from cells and high lipophilicity (4, 8). It may be necessary to examine whether the procedures for intracellular quantification of these agents (6, 7) suffer from the possible artifacts suggested for efavirenz in this study.

In conclusion, we have developed an intracellular efavirenz quantification method which overcomes spontaneous drug elution from cells and contamination with drug-containing plasma. The present method may be a useful tool for elucidating the therapeutic relevance of intracellular levels of efavirenz.

This study was supported by grants from the Ministry of Health, Labor and Welfare of Japan.

We thank Toshio Fukazawa for critical reading of the manuscript and gratefully acknowledge all the patients who participated in this trial.

REFERENCES

1. **Almond, L. M., P. G. Hoggard, D. Edirisinghe, S. H. Khoo, and D. J. Back.** 2005. Intracellular and plasma pharmacokinetics of efavirenz in HIV-infected individuals. J. Antimicrob. Chemother. **56:**738–744.
2. **Colombo, S., A. Beguin, A. Telenti, J. Biollaz, T. Buclin, B. Rochat, and L. A. Decosterd.** 2005. Intracellular measurements of anti-HIV drugs indinavir, amprenavir, saquinavir, ritonavir, nelfinavir, lopinavir, atazanavir, efavirenz and nevirapine in peripheral blood mononuclear cells by liquid chromatography coupled to tandem mass spectrometry. J. Chromatogr. B Analyt. Technol. Biomed. Life Sci. **819:**259–276.
3. **Csajka, C., C. Marzolini, K. Fattinger, L. A. Décosterd, J. Fellay, A. Telenti, J. Biollaz, and T. Buclin.** 2003. Population pharmacokinetics and effects of efavirenz in patients with human immunodeficiency virus infection. Clin. Pharmacol. Ther. **73:**20–30.
4. **Ford, J., S. H. Khoo, and D. J. Back.** 2004. The intracellular pharmacology of antiretroviral protease inhibitors. J. Antimicrob. Chemother. **54:**982–990.
5. **Gao, W.-Y., A. Cara, R. C. Gallo, and F. Lori.** 1993. Low levels of deoxynucleotides in peripheral blood lymphocytes: a strategy to inhibit human immunodeficiency virus type 1 replication. Proc. Natl. Acad. Sci. USA **90:** 8925–8928.
6. **Jones, K., P. G. Bray, S. H. Khoo, R. A. Davey, E. R. Meaden, S. A. Ward, and D. J. Back.** 2001. P-glycoprotein and transporter MRP1 reduce HIV protease inhibitor uptake in CD4 cells: potential for accelerated viral drug resistance? AIDS **15:**1353–1358.
7. **Jones, K., P. G. Hoggard, S. D. Sales, S. Khoo, R. Davey, and D. J. Back.** 2001. Differences in the intracellular accumulation of HIV protease inhibitors *in vitro* and the effect of active transport. AIDS **15:**675–681.
8. **Khoo, S. H., P. G. Hoggard, I. Williams, E. R. Meaden, P. Newton, E. G. Wilkins, A. Smith, J. F. Tjia, J. Lloyd, K. Jones, N. Beeching, P. Carey, B. Peters, and D. J. Back.** 2002. Intracellular accumulation of human immunodeficiency virus protease inhibitors. Antimicrob. Agents Chemother. **46:** 3228–3235.
9. **Marzolini, C., A. Telenti, L. A. Decosterd, G. Greub, J. Biollaz, and T. Buclin.** 2001. Efavirenz plasma levels can predict treatment failure and central nervous system side effects in HIV-1-infected patients. AIDS **15:** 71–75.
10. **Rotger, M., S. Colombo, H. Furrer, G. Bleiber, T. Buclin, B. L. Lee, O. Keiser, J. Biollaz, L. Décosterd, A. Telenti, and the Swiss HIV Cohort Study.** 2005. Influence of *CYP2B6* polymorphism on plasma and intracellular concentrations and toxicity of efavirenz and nevirapine in HIV-infected patients. Pharmacogenet. Genomics **15:**1–5.

Journal of General Virology (2007), 88, 2513–2519 DOI 10.1099/vir.0.82974-0

Increasing genetic diversity of hepatitis C virus in haemophiliacs with human immunodeficiency virus coinfection

Yasuhito Tanaka,[1] Kousuke Hanada,[2] Hideji Hanabusa,[3] Fuat Kurbanov,[1] Takashi Gojobori[2] and Masashi Mizokami[1]

Correspondence
Yasuhito Tanaka
ytanaka@med.nagoya-cu.ac.jp

[1]Department of Clinical Molecular Informative Medicine, Nagoya City University Graduate School of Medical Sciences, Kawasumi, Mizuho, Nagoya 467-8601, Japan

[2]National Institute of Genetics, Yata 1111, Mishima, Shizuoka, Japan

[3]Ogikubo hospital, Tokyo, Japan

Patients with inherited bleeding disorders who received clotting factor concentrates before 1987 have high rates of hepatitis C virus (HCV) or HCV/human immunodeficiency virus (HIV) infection. To determine whether the persistent nature of HIV affects the genetic diversity of HCV by less selective pressure through the immunosuppression of HIV/HCV-coinfected patients, both the change of genetic diversity and selective pressure were examined in the HCV envelope genes (E1 and E2) of 325 genotype 1a subclones from eight HIV-positive and five HIV-negative patients with two time points (more than 6 years apart). To infer the genetic diversity of HCV in each patient, we used two approaches. One method was to estimate the difference of total evolutionary distances in the phylogenetic tree between the two time points, and another was to estimate the changes of genetic diversity along the time based on the coalescence theory. The two results indicate that the HIV-positive group has significantly more diverse population structure than the HIV-negative group. A comparative analysis of the synonymous and non-synonymous substitutions found that the HIV-positive group was subject to less selective pressure than the HIV-negative group. In conclusion, HIV-positive patients would have a more diversified HCV population than HIV-negative patients due to less selective pressure from the immune system.

Received 6 March 2007
Accepted 3 May 2007

INTRODUCTION

Increased rates of progression to end-stage liver disease, mortality and reduced treatment response rates have been well documented in haemophiliac and other groups of chronic hepatitis C virus (HCV) carriers with human immunodeficiency virus (HIV) coinfection (Bica *et al.*, 2001; Goedert *et al.*, 2002; Braitstein *et al.*, 2004). Although the mechanism of liver disease progression in HIV-infected patients remains unclear, one of the important roles is assigned to immunosuppression (Goedert *et al.*, 2002).

The estimated HCV virion half-life time was, on average, 2.7 h with pre-treatment production and clearance of 10^{12} virions per day (Neumann *et al.*, 1998). Such a high rate of HCV replication, combined with lack of an error correction mechanism, results in the development of genetically diverse clones in a patient. The genetic diversity of HCV has provided critical insights into short-term outcomes, including early spontaneous viral clearance (Farci *et al.*, 2000), interferon-associated viral clearance (Farci *et al.*, 2002; Pawlotsky *et al.*, 1999) and HCV emergence following liver transplantation (Lyra *et al.*, 2002). To infer the genetic diversity of HCV in a patient, we applied two approaches. One method simply assumed that the genetic diversity of HCV is of different divergence of synonymous distance between two time points. The other method applied to coalescent analysis of genetic diversity along the time, assuming that the genetic diversity of HCV represents a heterogeneous viral population in a given carrier. To evaluate the influence on the HCV evolution exerted by the immunosuppression during persistent HIV coinfection, we examined a cohort of HCV carriers, comparing the HIV-positive and -negative groups.

Determination of the antigen-recognition regions associated with HCV-specific immune positive selection is important for understanding selective pressures underlying the evolution of HCV as well as putative therapeutic targets. In this study, we evaluated the genetic diversity of HCV and determined genomic regions associated with positive selection by comparative analysis of selective forces between HIV-positive and -negative groups in a cohort of haemophilia patients followed for more than 6 years.

The GenBank/EMBL/DDBJ accession numbers for the sequences reported in this study are AB245555–AB245873.